Journal of Energy Storage 152 (2026) 120541

Contents lists available at ScienceDirect

Journal of Energy Storage

journal homepage: www.elsevier.com/locate/est

Research Papers

A resilience-oriented multi-microgrid formation in distribution networks incorporating optimal allocation of mobile energy storages

Mohammad Toulabi [a], Mehdi Nikzad [b], Abouzar Samimi [c,d,*], Amin Samanfar [a]

[a] Department of Electrical Engineering, Khor. C., Islamic Azad University, Khorramabad, Iran
[b] Department of Electrical Engineering, Isl. C., Islamic Azad University, Islamshahr, Iran
[c] Department of Electrical Engineering, Arak University of Technology, Arak, Iran
[d] Department of Electrical Engineering, Bu-Ali Sina University, Hamedan, Iran

ARTICLE INFO

Keywords:
Resilience
Multi-microgrid
Energy storage systems
Utility function
Multi-objective
Mobile energy storage
Distributed energy resources

ABSTRACT

The increase in the number and severity of natural disasters and their significant social and economic effects have led power system operators and planners to pay special attention to enhancing the resilience of electricity distribution systems. Post-event restoration performance plays a critical role in improving the resilience of distribution systems. For this purpose, this paper presents an efficient mixed integer linear programming (MILP) model for improving the resilience of smart distribution networks based on a multi-objective approach. In the proposed framework, the distribution system is partitioned into several microgrids (MGs) using distributed generators (DGs), Energy Storage Systems (ESSs), controllable switches, as well as smart grid technologies, and, simultaneously, the optimal placement of Mobile Energy Storage (MES) units is determined to enhance system resilience. In the first objective function, the total utility functions, and consequently the social welfare of network loads in the restoration process should be maximized. On the other hand, the restoration cost including operational cost of generation units and charging and discharging costs of ESSs and MESs as the second objective function is minimized. The proposed multi-objective model is solved using the ε-constraint method in the GAMS environment based on the CPLEX solver, and the optimal solution is obtained using a fuzzy decision-making procedure. Finally, in order to confirm the effectiveness of the proposed method in improving the resilience of smart distribution systems, the proposed model is successfully examined on the IEEE 33-bus distribution network under two different disaster scenarios. The obtained results indicate that the optimal Pareto point provides a balanced solution with welfare of 245,431.48 and a cost of $333,305, achieving over 99.9% of maximum possible welfare while keeping cost near the minimum.

1. Introduction

1.1. Background and literature review

In recent years, the increasing severity and frequency of unavoidable natural disasters—driven by climate change—have significantly impacted power systems. Therefore, enhancing the resilience of electric power distribution networks has garnered significant research attention due to the increasing frequency and severity of extreme events that threaten power supply continuity [1]. Extreme disasters with small probability and high loss have led to more frequent and intense power outages, particularly in distribution systems [2]. The devastating impact of high-impact rare natural events on power systems has prompted researchers to investigate technologies and infrastructure aimed at enhancing power system resilience. Therefore, effective resilience enhancement strategies encompassing both pre-disaster network hardening measures and post-disaster restoration schemes are essential for ensuring the reliability and adaptability of modern power systems. [3].

Numerous studies have focused on restoring distribution systems by rescheduling resources and reconfiguring network structures to recover critical loads after disruptive events and natural disasters. However, during natural disasters, the upstream network or the main grid may be out of service, requiring the distribution system to operate in an islanded mode. In these scenarios, conventional operational strategies often fall short in ensuring continuous a power supply. To address this challenge, integrating distributed energy resources (DERs) and smart grid solutions, such as demand response (DR) programs, can significantly

* Corresponding author at: Department of Electrical Engineering, Arak University of Technology, Arak, Iran.
E-mail addresses: mohammad.toulabi1990@iau.ac.ir (M. Toulabi), mehdi.nikzad@iau.ac.ir (M. Nikzad), a.samimi@arakut.ac.ir, a.samimi@basu.ac.ir (A. Samimi), a.samanfar@iau.ac.ir (A. Samanfar).

https://doi.org/10.1016/j.est.2026.120541
Received 7 September 2025; Received in revised form 31 December 2025; Accepted 12 January 2026
Available online 28 January 2026
2352-152X/

Nomenclature

Acronyms

MG Microgrid
ESS Battery Energy Storage System
MES Mobile Battery Energy Storage
DG Distributed Generation
VOLL Value Of Lost Load

Indices and sets

i, j, r index of buses.
ij index of lines from bus i to bus j.
b index of MES.
ψ Index of scenarios for active power production of PVs.
$\boldsymbol{N}$ Set of buses (nodes).
$\boldsymbol{\Omega}$ Set of scenarios.
$\boldsymbol{L}$ Set of distribution lines $l = (i,j)$.
$\boldsymbol{MES}$ Set of MES.
$\boldsymbol{M}$ Set of potential MGs.
$\boldsymbol{MCDG}$ Set of buses connected to DGs with master control capabilities.
$\boldsymbol{T}$ Hours from 1 to T.

Variables and parameters

$z_{i,m}$ Binary variable: 1 if bus i is assigned to MG m, 0 otherwise.
$\gamma_{r,m}$ Binary variable: 1 if DG at bus $r \in \boldsymbol{MCDG}$ is the master unit of MG m, 0 otherwise.
y_{ij} Binary variable: 1 if the line between buses i and j is used, 0 otherwise.
$a_{ij,m}$ Binary variable: 1 if line (i,j) belongs to MG m, 0 otherwise.
$active\_MG_m$ Binary variable: 1 if MG m is formed, 0 otherwise.
s_{ij} Binary variable: 1 if line (i,j) is available, 0 otherwise (damaged).
s_i Binary variable: 1 if bus i is available, 0 otherwise (damaged).
$f_{ij,m}$ Positive variable indicating virtual power flow from bus i to j in MG m.
$X_{b,i}$ Binary variable: 1 if MES b is connected to bus i, otherwise 0.
$P^{ESS}_{dch,i,t,\psi}$ Discharging power of ESS in bus i, at hour t, and in scenario ψ.
$P^{ESS}_{ch,i,t,\psi}$ Charging power of ESS in bus i, at hour t, and in scenario ψ.
$E^{ESS}_{i,t,\psi}$ State of Charge (SOC) of ESS in bus i, at hour t, and in scenario ψ.
$E^{ESS}_{i,initial}$ Initial SOC of ESS in bus i.
$\eta^{ESS}_{ch,i}$, $\eta^{ESS}_{dch,i}$ Charging/Discharging efficiency of ESS in bus i.
$E^{ESS}_{i,min}$, $E^{ESS}_{i,max}$ Minimum/Maximum allowable SOC of ESS in bus i.
$u^{ESS}_{ch,i,t}$, $u^{ESS}_{dch,i,t}$ Binary variable representing charging/discharging status of ESS in bus i, at hour t, and in scenario ψ.
$f_b(\xi)$ Beta Probability Distribution Function (PDF) of solar irradiance (ξ)
$P^{DG}_{i,t,\psi}$ Scheduled active power of DG in bus i, at hour t, and in scenario ψ.
$P^{PV}_{i,t,\psi}$ Scheduled power output of PV in bus i, at hour t, and in scenario ψ.
$P^{DG}_{i,min}$, $P^{DG}_{i,max}$ Minimum/Maximum power generation of DG at bus i.
$P^{MES}_{dch,b,t,\psi}$ Discharging power of MES b, at hour t, and in scenario ψ.
$P^{MES}_{ch,b,t,\psi}$ Charging power of MES b, at hour t, and in scenario ψ.
$P^{d}_{i,t,\psi}$ Consumed power by loads in bus i, at hour t, and in scenario ψ during post-event.
$P^{Load}_{i,t}$ Normal load demand in bus i, at hour t.
$E^{MES}_{b,t,\psi}$ SOC of MES b, at hour t, and in scenario ψ.
$E^{MES}_{b,initial}$ Initial SOC of MES b.
$\eta^{MES}_{ch,b}$, $\eta^{MES}_{dch,b}$ Charging/Discharging efficiency of MES b.
$E^{MES}_{b,min}$, $E^{MES}_{b,max}$ Minimum/Maximum allowable SOC of MES b.
$u^{MES}_{ch,b,t,\psi}$, $u^{MES}_{dch,b,t,\psi}$ Binary variable representing charging/discharging status of MES b, at hour t, and in scenario ψ.
$g_{m,b,i}$ Auxiliary variable to linearize the multiplication of two variables.
$U(x, \omega)$ Utility function of a consumer (load) with x load's power consumption level and parameter ω
π_t Energy price (tariff rate) at hour t.
$U_i\left(P^{d}_{i,t,\psi}\right)$ utility function of load at bus i with power consumption of $P^{d}_{i,t,\psi}$.
ρ_ψ Probability of considered scenarios for active power production of PVs.
$m^1_{i,t,\psi}, m^2_{i,t,\psi}, m^3_{i,t,\psi}$ Binary variables indicating that the utility function of load in bus i, at hour t, and in scenario ψ is located in only one of three defined segments.
$\delta^1_{i,t,\psi}, \delta^2_{i,t,\psi}, \delta^3_{i,t,\psi}$ Positive variable representing the activated level at each of three defined segments in the utility function of load in bus i, at hour t, and in scenario ψ.
α^1_i, α^2_i, α^3_i maximum load consumption level in bus i, in segments 1, 2 and 3 as a percentage of the total maximum load
$u1_i$, $u2_i$, $u3_i$ Slope of the utility function of load in bus i in segments 1, 2, and 3.
$Price^{DG}_{i,t}$ Price of power generation by DG in bus i at hour t.
$Price^{PV}_{i,t}$ Price of power production by PV unit in bus i at hour t.
$Price^{ESS}_{i,t}$ Cost of charging/discharging of ESS in bus i at hour t.
$Price^{MES}_{b,t}$ Cost of charging/discharging of MES b at hour t.
$VOLL^{shed}_{i,t}$ value of lost load in bus i at hour t.

enhance system resilience by improving the ability to restore loads [4]. With the growing integration of DERs, forming microgrids (MGs) has emerged as an effective strategy for restoring critical loads during major power outages in distribution networks. To address the MG formation model in the resiliency of distribution networks, researchers have applied both heuristic optimization approaches [5–8] and mathematical programming techniques [9–13]. In the context of heuristic optimization methods, a graph theory-based methodology along with the Choquet integral has been presented in [5] to support MG formation, and distribution system resilience under extreme contingencies has been evaluated. The authors of [6] have proposed a heuristic method capable of addressing the post-event MG formation problem in medium to large-scale power systems. Similarly, a resilience-oriented framework is developed in [7] to use MGs to restore critical loads following major outages, while incorporating MG stability and technical constraints such as transient currents, voltage limits of DGs, and allowable frequency deviations. In [8], a metaheuristic algorithm was introduced for optimal operation of smart distribution networks for MG formation with DERs, although this model did not consider DR programs. Authors of [14] have formulated a MG formation model that integrates voltage, power loss, and power balance constraints, employing mixed-integer linear programming (MILP) based on exact power flow equations. A chance-constrained optimization model is presented in [9] to determine the most suitable partitions for MG formation in response to natural events.

Different control strategies can be applied to DGs, each leading to distinct operational outcomes during system restoration. One commonly used approach is the droop-control method, which enables decentralized operation without requiring communication between DG units [15]. However, a key limitation of this method is the occurrence of circulating currents among DGs. To address this issue, the master-slave control strategy has been introduced. In this approach, a designated master DG unit regulates the system's voltage and frequency, while the remaining DGs operate in current control mode as slave units [10–13]. This master-slave configuration has been widely adopted in MG formation studies aimed at enhancing distribution system resilience. Authors of [10] have introduced a MILP model for critical load recovery through MG formation and optimal management of DERs after extreme events. In [12], a two-stage optimization framework has been proposed to improve system resilience post high-impact events using DERs. Also, authors in [11] have developed a single-objective model focused on MG formation using electric vehicles (EVs) and direct load control to restore critical loads. This approach significantly improved computational efficiency by reducing the number of binary and continuous variables. A bi-level optimization model based on the master-slave technique has been proposed in [13] to enhance distribution system resilience following natural disasters, incorporating the role of fast-charging stations. The lower level models the dynamic charging demand of operational stations considering transportation network constraints, while the upper level determines island boundaries to maximize load restoration.

Implementing DR programs significantly enhances the resilience of distribution systems during natural disasters. By shedding or shifting non-critical loads based on agreements between consumers and the DSO, critical loads can be restored more efficiently. In [16], authors have proposed a post-event restoration model that improves system resilience by incorporating DERs, while critical and interruptible loads within a DR framework are used to strengthen post-event resilience of distribution systems. A framework for resilient distribution service restoration is introduced in [17] by utilizing integrated control of household flexible appliances to shape the demand curve. However, the study did not incorporate dynamic MG formation for restoring critical loads following natural events, nor did it consider restoration cost as an objective in implementing DR programs.

One of the key tools employed in multi-energy systems to enhance system resiliency is the use of mobile energy providers. The concept of mobile generation is a highly effective tool for meeting energy demand during critical situations [18]. In post-disaster scenarios, various types of mobile generation units can be utilized, including:

Mobile Energy Storage (MES): Battery energy storage systems (BESS) enhance system resilience by supplying localized electrical support during outages. Moreover, mobile storage units enable continued utilization of renewable energy sources during disruptions and help optimize fuel usage by extending the operating time of emergency generators [19].

Mobile Generator Units: Mobile generators powered by natural gas or diesel are designed for easy transportation and rapid deployment during unexpected emergencies.

Transportable Renewable Energy Generators: Mobile renewable energy sources, such as portable PV units, offer a reliable power solution in remote locations and under unpredictable conditions [20].

1.2. State of the art and motivation

Recent advancements in smart grid research have increasingly focused on leveraging *MES systems* and *dynamic MG formation* to enhance distribution network resilience under extreme events. For example, authors of Ref. [21] have proposed adaptive MG formation frameworks to improve post-disaster resilience while reducing computational burden. By reformulating power flow equations using graph-theoretic single-commodity flow concepts, these approaches eliminate the need for predefined MG roots and topologies, enabling scalable and efficient modeling under large-scale deployment of mobile energy resources. Numerical results on large benchmark systems demonstrate that such adaptive formulations significantly enhance computational tractability while maintaining accurate load restoration performance. Ref. [22] has emphasized the importance of considering interdependencies among power, transportation, and information networks (PTINs) in post-disaster restoration. By integrating MES systems, electric vehicles, and unmanned aerial vehicles into a rolling optimization framework, these studies demonstrate that coordinated recovery across interconnected infrastructures can substantially improve restoration speed and recovered load levels. However, such approaches primarily focus on infrastructure interdependency modeling and dynamic recovery sequencing, rather than integrated MG formation and welfare-driven load prioritization. In [23], the authors have addressed the integration of battery degradation considerations into MES units scheduling, balancing operational resilience with long-term asset performance. Specific scheduling strategies have also been developed in [24] to optimize MES systems deployment for resilience enhancement under severe weather conditions such as ice storms. A two-stage optimization framework has been developed to determine both the optimal allocation and routing of MES units under weather-induced line failure risks.

Beyond purely post-disaster models, comprehensive disaster management frameworks have been introduced in [25] that jointly address pre-disaster preparedness and post-disaster recovery using MES systems. These approaches combine robust pre-event deployment with dynamic post-event scheduling to cope with renewable generation uncertainty and time-varying system conditions. A restoration approach based on forming MGs and deploying mobile emergency generators, using Deep Q-Network (DQN) as an algorithm of deep reinforcement learning has been proposed [26] to optimize load recovery and ensure high reliability for critical loads.

The inclusion of electric vehicles as MES assets in post-typhoon restoration further demonstrates emerging hybrid restoration strategies that exploit mobile flexibility to reduce load shedding and economic losses [27]. A growing body of research explores the role of MES systems and other mobile resources in improving distribution network resilience under severe contingencies. For instance, adaptive robust load restoration approaches that coordinate distribution network reconfiguration with MES have been developed in [28], demonstrating improved restoration performance during unforeseen outages. Further work in distribution network contexts, such as port distribution, has examined resilience enhancement through pre-deployment and dynamic scheduling of MES systems alongside DGs [29]. Additionally, models that optimize the placement and management of MES in active networks have been shown to reduce generation deficit and improve operational survivability of distribution systems following outages [30]. Research has also explored the resilience and sustainability gains of emergency operation of truck-mounted mobile battery energy storage fleets, which can support critical loads and improve post-event system performance [31]. Moreover, multi-MG frameworks that integrate MES units and parking lot resources have been introduced to enhance coordinated resource sharing and resilience against infrastructure damage and widespread outages [32].

A methodology for estimating resiliency in multi-energy MGs has been presented in [33], emphasizing the crucial role of mobile energy providers in mitigating the devastating impacts of natural disasters. These mobile units can significantly improve system resiliency by supplying energy where and when it is most needed during emergencies. The proposed approach evaluates resiliency based on the cost of unserved energy, which reflects the economic impact of energy outages caused by natural disasters in multi-energy MGs. To tackle the challenge of communication system unavailability and enhance the coordinated restoration of transmission and distribution systems after extreme disasters, a multi-period distributionally robust resilience enhancement model is introduced in [34] for a jointly transmission-distribution network. The presented model involves pre-disaster rental and strategic deployment of MES units to support critical loads and maintain power balance throughout the restoration process and unmanned aerial vehicles to mitigate communication failures caused by natural disasters and facilitate information exchange. Ref. [35] has proposed an MES planning model focused on maximizing the profitability of DSOs during power outages. In [36], a bi-level optimization approach is introduced for enhancing distribution system resilience to extreme disasters using MES. Authors of Ref. [37] have introduced a three-stage stochastic distributed control algorithm aimed at improving MG resilience with MES. Ref [38] has developed a coordinated energy scheduling model tailored for highway energy demand scenarios using MES. The concept of mobile compressed air energy storage to boost distribution grid performance is presented in [39]. Ref. [40] explored the joint optimization of MES, power systems, and transportation networks to support greater integration of renewable energy sources. A bi-level optimization framework for MES in active distribution systems is presented in [41], focusing on revenue maximization through location marginal pricing settlement. The upper level optimizes MES capacity, routing, and dispatch, while the lower level jointly clears energy and reserve markets and optimizes renewable integration using AC optimal power flow.

MESs in power networks offer a highly adaptable solution for balancing supply and demand at any bus. Their rapid deployment and operational efficiency make them especially valuable during natural disasters, as they can be quickly relocated among neighboring buses. This capability is particularly critical for essential infrastructure, such as local hospitals and emergency command centers, where MES units can deliver fast response, real-time voltage control, and multiple services, including energy arbitrage, voltage regulation, and reactive power support. These functions help ensure voltage stability and an uninterrupted power supply at vital nodes. Despite their potential, recent research on utilizing MES for enhancing power system resilience remains limited. Therefore, according to the above explanation, developing an effective model and dispatch strategy for dynamic MG formation integrated with optimal location of MES during the post-disaster stage deserves significantly greater attention at present. For such motivations and research gaps, in this paper, an efficient model for integrated MG formation and optimal allocation of the MES units is presented based on the maximization of total welfare (or total utility functions) of consumers as coordinated operational strategies for service restoration. Moreover, there remains a gap in the literature regarding a comprehensive mathematical formulation that simultaneously addresses the multi-objective optimization of load restoration and operational costs following extreme events. To address these gaps, this paper introduces a cost-restoration stochastic optimization model formulated as a Mixed-Integer Linear Programming (MILP) problem.

In Table 1, the proposed model is compared with the relevant existing studies cited in the manuscript, highlighting its novelty and advantages in welfare-based load prioritization, coordinated MES deployment, and multi-objective post-disaster restoration.

The main contributions of the proposed approach are as follows:

- A novel consumers' welfare-based optimization model is proposed to form post-disaster MGs by prioritizing loads based on the consumers' utility function, rather than only demand size.
- MES units are optimally allocated to enhance network resilience, considering their flexible relocation and operation.
- A multi-objective ε-constraint approach is employed to compromise total utility functions maximization and operational cost minimization, providing a Pareto-efficient solution set.

The remainder of this paper is organized as follows: model outline is presented in Section 2. Section 3 describes the problem formulation of the proposed model. The simulation results and discussion are provided in Section 4 to investigate various aspects of the proposed model. Finally, the conclusions of the paper are outlined in Section 5.

2. Model outline

Fig. 1 presents the overall framework of the proposed post-event restoration model tailored for smart distribution networks impacted by natural event outages. In the first stage, damaged lines and buses are systematically identified through the coordinated deployment of advanced sensing, protection, and communication devices. Intelligent switching devices, such as automated reclosers and sectionalizers, are typically equipped with local sensing capabilities and Remote Terminal Units (RTUs), thereby enabling real-time fault detection and automated isolation. These devices report system events and status to the central control center via Supervisory Control and Data Acquisition (SCADA) systems, which provide operators with a comprehensive view of network conditions and facilitate remote operation. In addition, Advanced Metering Infrastructure (AMI) and Phasor Measurement Units (PMUs) further enhance observability by supplying granular voltage, current, and phase angle data. The data collected from these distributed devices is analyzed using fault detection, isolation, and restoration algorithms to support rapid and intelligent system restoration. Subsequently, Stage 2 delineates the schedulable zone—defined as the subset of buses and feeders electrically isolated from the upstream grid—where MG formation is feasible. Within this framework, the distribution network is strategically separated into multiple MGs by leveraging DG units and intelligent switching technologies. Accordingly, Stage 3 formulates a multi-objective optimization problem that accounts for both structural and operational constraints associated with MG deployment, while incorporating advanced smart grid functionalities, such as MESs. The mathematical formulation of the objective functions and corresponding constraints in Stage 3 is detailed in Section 3.

The proposed framework is developed based on several simplifying assumptions that are commonly adopted in resilience-oriented restoration studies. It is assumed that reliable and delay-free communication exists among the distribution system operator (DSO), DERs, and smart grid devices, enabling centralized coordination during the restoration process. In addition, the relocation and connection of MES units are assumed to be instantaneous, without explicitly modeling transportation network constraints or travel times. Static line ratings and steady-state operation are considered. These assumptions allow the formulation to remain computationally tractable and suitable for post-event decision support. Nevertheless, relaxing these assumptions and incorporating more detailed communication, transportation, and dynamic network models constitute promising directions for future research.

3. Problem formulation

3.1. Uncertainty modeling of renewable-based DGs

Due to the inherent variability of solar resources, the power output of these units is inherently intermittent. Here, a scenario-based stochastic programming approach has been utilized to model the uncertainty associated with solar irradiation. The output power of a PV unit primarily depends on solar irradiance. At a given location, hourly irradiance typically exhibits a bimodal distribution, which can be represented as a linear combination of two unimodal distributions. Each unimodal component is modeled using a Beta probability distribution function (PDF), as given below [42]:

$$f_b(\xi) = \begin{cases} \dfrac{\Gamma(\alpha+\beta)}{\Gamma(\alpha)\Gamma(\beta)}\xi^{\alpha-1}(1-\xi)^{\beta-1} & 0 \le \xi \le 1, \alpha \ge 0, \beta \ge 0 \\ 0 & otherwise \end{cases} \tag{1}$$

Here, ξ represents the solar irradiance in kW/m^2, and $f_b(\xi)$ denotes the Beta distribution function of ξ, with α and β as its shape parameters. To determine these parameters, the mean μ and standard deviation σ of the random variable s are used, as shown below [42]:

Table 1
The summary of the literature review.

Ref.	Welfare-based load prioritization	Single/multi-objective	Mobile energy storage (MES)	Coordination: MES allocation and MG formation	Optimization method	Uncertainty/risk modeling	Key limitations/remarks
[5]	x	Single	x	x	Graph theory + Choquet integral	x	Heuristic, no MES or welfare function
[6]	x	Single	x	x	Heuristic	Stochastic pre-disturbance	No DR, limited DER consideration
[7]	x	Single	x	x	Heuristic	x	MG formation only, no MES
[8]	x	Single	x	x	Metaheuristic	x	Active distribution network self-healing, no MES
[9]	x	Single	x	x	Chance-constrained	Event uncertainty	No MES, welfare not considered
[10]	x	Single	x	Partial	MILP	x	DER integration, no MES or welfare
[11]	x	Single	x	x	MILP	x	EVs for restoration, no multi-objective welfare
[12]	x	Multi	x	Partial	Two-stage stochastic MILP	Scenario-based	EVs integrated, no MES dynamic relocation
[13]	x	Single	x	Partial	Bi-level MILP	x	EV charging stations considered, welfare not included
[14]	x	Single	x	x	Exact MILP	x	Microgrid formation with DERs, no MES
[16]	x	Single	x	x	Linear topological + DER scheduling	x	No MES, welfare not included
[17]	x	Single	x	x	DR-based restoration	x	Focus on demand response, no MES or welfare
[21]	x	Multi	✓	Partial	Adaptive MG formation	x	MES deployment, no welfare-based load prioritization
[22]	x	Multi	✓	Partial	Rolling optimization	PTIN interdependencies	Coordination is limited, no welfare function
[23]	x	Multi	✓	Partial	MILP	Battery degradation	Focused on MES scheduling, no welfare prioritization
[24]	x	Multi	✓	Partial	Two-stage MILP	Weather-induced failures	MES scheduling under an ice storm, no welfare
[25]	x	Multi	✓	Partial	Disaster management framework	x	Pre/post-disaster MES, welfare not considered
[26]	x	Multi	✓	Partial	Deep RL (DQN)	x	Restoration with mobile generators, welfare not included
[27]	x	Multi	✓	Partial	MILP	x	EV + MES coordination, no welfare-based prioritization
[28]	x	Multi	✓	Partial	MILP + Robust	x	Adaptive load restoration, no welfare function
[29]	x	Multi	✓	Partial	MILP	x	Port distribution networks, welfare not included
[30]	x	Multi	✓	Partial	MILP	x	MES management optimization, no welfare
[31]	x	Multi	✓	Partial	Emergency operation model	x	Truck-mounted MES, no welfare prioritization
[32]	x	Multi	✓	Partial	Multi-MG framework	x	MES + MG, coordination limited, no welfare
[36]	x	Multi	✓	Partial	Bi-level MILP	x	MES spatial-temporal flexibility, no welfare
[37]	x	Multi	✓	Partial	Stochastic distributed control	x	MG network control, no welfare prioritization
[38]	x	Multi	✓	Partial	DMPC optimization	x	Highway microgrid scenarios, welfare not included
[40]	x	Multi	✓	Partial	MILP + AC OPF	x	MES + transport integration, no welfare
[41]	x	Multi	✓	Partial	Bi-level MILP	x	Revenue maximization via MES, welfare not prioritized
This paper	✓ (Maximizes total utility)	Multi	✓	Full coordination (MES + MG formation)	MILP + ε-constraint + fuzzy decision-making	Stochastic (post-disaster)	Maximizes welfare & restores critical loads efficiently, balances cost and resilience

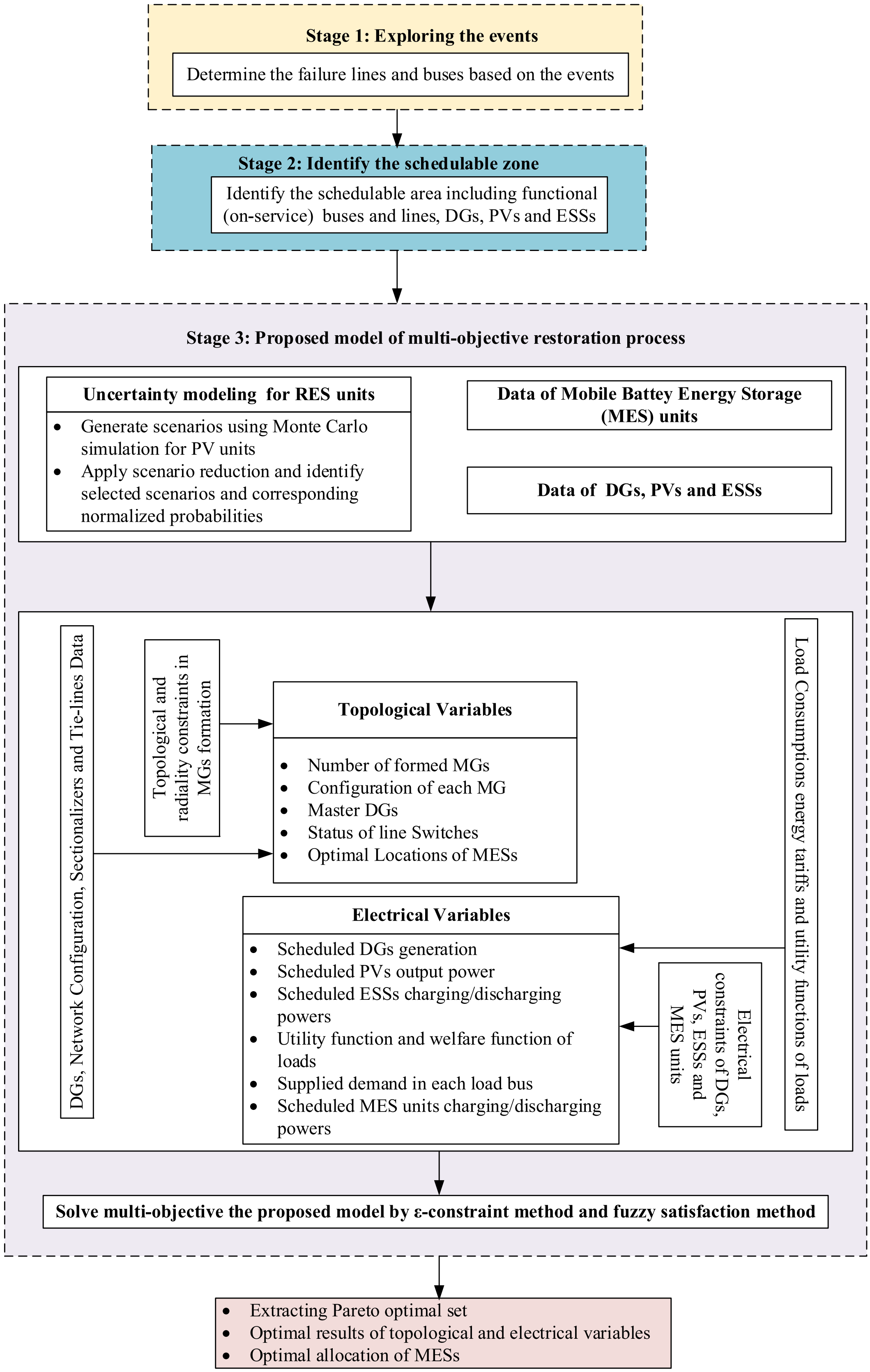

Fig. 1. Overall framework for the proposed model.

$$\beta = (1-\mu)\times\left(\frac{\mu\times(1+\mu)}{\sigma^2}-1\right) \tag{2}$$

$$\sigma = \frac{\mu\times\beta}{1-\mu} \tag{3}$$

The continuous PDF of the uncertain parameter is discretized into five intervals with a specific range for solar irradiance. Considering that PV generation occurs mainly between hours 6 and 19 (a total of 14 h), and assuming a discretized PDF with five intervals, a total of 5^{14} scenarios are generated according to the scenario tree model. This value represents the theoretical size of the complete scenario tree and is mentioned only to highlight the computational intractability of directly modeling all possible realizations. In practice, however, such a large scenario set is not constructed explicitly. Instead, 1000 daily PV generation trajectories over a 24-hour horizon are generated using Monte Carlo simulation. Each trajectory represents a single coherent realization of PV output across the entire scheduling horizon, rather than independent hourly scenarios. Therefore, it is essential to apply an effective scenario reduction technique to ensure that the system's uncertain behavior is accurately approximated while keeping the problem computationally manageable. Backward scenario reduction is an efficient approach provided in [43]. This technique generates a reduced set of scenarios that effectively approximates the original scenario set.

Since the focus of this work is on post-disaster restoration and resilience assessment rather than site-specific PV forecasting, typical Beta distribution parameters reported in prior studies are employed. Specifically, the solar irradiance is normalized in the range [0,1] and modeled using a Beta distribution with shape parameters $\alpha = 2.5$ and $\beta = 4.5$, corresponding to a mean value $\mu \approx 0.36$ and standard deviation $\sigma \approx 0.18$. These values represent moderate solar conditions and have been commonly used in scenario-based stochastic studies of PV generation. The generated irradiance samples are subsequently converted into PV power outputs and used to construct Monte Carlo scenarios, which are then reduced using a backward scenario reduction technique.

3.2. Topological and radiality constraints in MGs formation

Severe natural disasters or extreme weather events can disrupt distribution networks, rendering them incapable of receiving power from the main grid. In such cases, DGs within MGs can facilitate local power restoration by supplying electricity to critical loads until the main grid connection is re-established. In this section, graph-theoretic concepts and their relationships are employed to model the topological and radiality constraints of MG formation. In the proposed model, a comprehensive network graph encompassing all buses and lines is constructed. Due to the inclusion of tie lines, the resulting graph inherently contains multiple loops. Additionally, in a master-slave control framework, a single DG operates as the master unit, responsible for regulating the MG voltage and frequency, while the remaining DG units function as slave units, adjusting their output to follow the established voltage and frequency. Consequently, the maximum number of *potential* MGs is equal to the number of master-control DGs. It is assumed that all active lines are equipped with controllable switches. The processes of MG formation and network topology reconfiguration rely on the opening and closing of these switches.

a) *Buses assignment to MGs*

- A bus can be assigned to a MG only if it is available, as given by Eq. (4):

$$z_{i,m} \le s_i \forall i \in \boldsymbol{N}, \forall m \in \boldsymbol{M} \tag{4}$$

Eq. (4) prevents damaged buses from being assigned to any MG.

- Due to technical constraints, each available bus can be assigned to exactly one MG or remain unassigned. Thus, the following constraint is imposed:

$$\sum\nolimits_{m\in \boldsymbol{M}} z_{i,m} \le 1 \forall i \in \boldsymbol{N} \tag{5}$$

Should the variable $z_{i,m}$ equals 1, it indicates that bus i belongs to MG m.

- A bus can be assigned to MG m only if the MG is activated as given by Eq. (6):

$$z_{i,m} \le active\_MG_m \forall i \in \boldsymbol{N}, \forall m \in \boldsymbol{M} \tag{6}$$

b) *Lines assignment to MGs*

- A Line can be used in a MG only if it is available, as expressed by Eq. (7):

$$y_{ij} \le s_{ij} \forall (i,j) \in \boldsymbol{L} \tag{7}$$

- A line can be assigned to a MG only if both ends are assigned to that MG and the line is functional:

$$a_{ij,m} \le z_{i,m}, a_{ij,m} \le z_{j,m}, a_{ij,m} \le s_{ij} \forall (i,j) \in \boldsymbol{L}, \forall m \in \boldsymbol{M} \tag{8}$$

$$\sum_{m\in \boldsymbol{M}} a_{ij,m} = y_{ij} \forall (i,j) \in \boldsymbol{L} \tag{9}$$

c) *Constraints on MG formation*

- Each MG has at least one master DG as follows:

$$\sum_{r\in \boldsymbol{MCDG}} \gamma_{r,m} \ge active\_MG_m \forall m \in \boldsymbol{M} \tag{10}$$

d) *Radiality and connectivity constraints for each MG based on artificial power flow*:

To ensure a radial topology within each islanded MG, this study employs the concept of Artificial Power Flow (APF), a widely adopted technique in linear programming formulations of distribution networks. The APF method circumvents this issue by introducing auxiliary continuous variables representing fictitious flow between nodes. In the proposed model, each MG is treated as a subgraph rooted at a single master control unit, which serves as the origin of an artificial power flow. All other buses assigned to that MG act as sink nodes, each demanding one unit of the fictitious power. The artificial flow is not related to real power or energy exchange but is merely a mathematical tool to enforce the radial (tree-like) structure [44,45].

The formulation relies on the following key principles:

- Radiality enforcement: Since a tree with n nodes has exactly n − 1 edges (lines), limiting the number of active lines ensures the absence of cycles.
- Flow conservation: Each non-root bus must receive exactly one unit of flow, implying it is connected through a valid path to the root.
- Root injection: The master unit injects a total flow equal to the number of sink buses.
- Binary activation: Artificial flow through a line is allowed only if the line is active in the MG's topology (enforced via Big-M constraints).

According to APF explanation, the following equations are used to ensure the radial structure and eliminate loops within each MG.

$$\sum_{(i,j)\in \boldsymbol{L}} a_{ij,m} = \sum_{i\in \boldsymbol{N}} z_{i,m} - active\_MG_m \forall m \in \boldsymbol{M} \tag{11}$$

Each tree contains a number of edges (lines) equal to the number of nodes minus one, which ensures a radial structure. This constraint also guarantees that if a MG is inactive, no buses are assigned to it. Flow conservation can be written as follows:

$$\sum_{j:(i,j)\in \boldsymbol{L}} f_{ij,m} - \sum_{j:(j,i)\in \boldsymbol{L}} f_{ji,m} = z_{i,m} - \gamma_{i,m} \forall i \in \boldsymbol{N}, \forall m \in \boldsymbol{M} \tag{12}$$

$$f_{ij,m} \leq a_{ij,m}.BigM \tag{13}$$

It should be noted that the artificial power flow formulation relies on Big-M constraints to link line activation variables with the fictitious flow variables. In this study, the Big-M parameter is selected based on the maximum possible artificial flow within each MG. Since each non-root bus requires exactly one unit of fictitious flow and the number of buses in a MG cannot exceed the total number of network buses, the Big-M value is conservatively set equal to the total number of buses in the system. The detailed explanations about aforementioned equations are provided in [46–48].

3.3. Electrical constraints in MGs formation

All power-related variables in the model are expressed in kW and are assumed to be constant over each scheduling time interval. The optimization horizon is discretized into hourly time steps ($\Delta t = 1$ h). Therefore, power balance constraints are formulated in kW, while the state-of-charge (SOC) equations implicitly account for Δt, ensuring dimensional consistency between power (kW) and energy (kWh).

- Power balance in each isolated MG:

$$\sum_{i\in \boldsymbol{N}} z_{i,m}\left(P^{DG}_{i,t,\psi} + P^{PV}_{i,t,\psi} + P^{ESS}_{dch,i,t,\psi} - P^{ESS}_{ch,i,t,\psi} + \sum_{b\in \boldsymbol{MES}}\left(P^{MES}_{dch,b,t,\psi}\cdot X_{b,i} - P^{MES}_{ch,b,t,\psi}\cdot X_{b,i}\right)\right) = \sum_{i} z_{im}\cdot P^{d}_{i,t,\psi} \forall m \in \boldsymbol{M}, \forall t \in \boldsymbol{T}, \forall \psi \in \boldsymbol{\Omega} \tag{14}$$

- Constraints of DGs, PV units and ESSs:

$$P^{DG}_{i,min}\cdot s_i \leq P^{DG}_{i,t,\psi} \leq P^{DG}_{i,max}\cdot s_i \forall i \in \boldsymbol{N}, \forall t \in \boldsymbol{T}, \forall \psi \in \boldsymbol{\Omega} \tag{15}$$

$$0 \leq P^{PV}_{i,t,\psi} \leq P^{PV}_{i,\psi,max}\cdot s_i \forall i \in \boldsymbol{N}, \forall t \in \boldsymbol{T}, \forall \psi \in \boldsymbol{\Omega} \tag{16}$$

$$E^{ESS}_{i,t,\psi} = E^{ESS}_{i,initial} + P^{ESS}_{ch,i,t,\psi}\cdot \eta^{ESS}_{ch,i} - \frac{P^{ESS}_{dch,i,t,\psi}}{\eta^{ESS}_{dch,i}} \forall i \in \boldsymbol{N}, \forall \psi \in \boldsymbol{\Omega}, t = 1 \tag{17}$$

$$E^{ESS}_{i,t,\psi} = E^{ESS}_{i,t-1,\psi} + P^{ESS}_{ch,i,t,\psi}\cdot \eta^{ESS}_{ch,i}\cdot \Delta t - \frac{P^{ESS}_{dch,i,t,\psi}\cdot \Delta t}{\eta^{ESS}_{dch,i}} = E^{ESS}_{i,t-1,\psi} + P^{ESS}_{ch,i,t,\psi}\cdot \eta^{ESS}_{ch,i} - \frac{P^{ESS}_{dch,i,t,\psi}}{\eta^{ESS}_{dch,i}} \forall i \in \boldsymbol{N}, \forall \psi \in \boldsymbol{\Omega}, t \geq 2 \tag{18}$$

$$E^{ESS}_{i,min} \leq E^{ESS}_{i,t,\psi} \leq E^{ESS}_{i,max} \forall i \in \boldsymbol{N}, \forall t \in \boldsymbol{T}, \forall \psi \in \boldsymbol{\Omega} \tag{19}$$

$$P^{ESS}_{ch,i,t,\psi} \leq P^{ESS}_{i,max}\cdot u^{ESS}_{ch,i,t,\psi}\cdot s_i \forall i \in \boldsymbol{N}, \forall t \in \boldsymbol{T}, \forall \psi \in \boldsymbol{\Omega} \tag{20}$$

$$P^{ESS}_{dch,i,t,\psi} \leq P^{ESS}_{i,max}\cdot u^{ESS}_{dch,i,t,\psi}\cdot s_i \forall i \in \boldsymbol{N}, \forall t \in \boldsymbol{T}, \forall \psi \in \boldsymbol{\Omega} \tag{21}$$

$$u^{ESS}_{ch,i,t,\psi} + u^{ESS}_{dch,i,t,\psi} \leq 1 \forall i \in \boldsymbol{N}, \forall t \in \boldsymbol{T}, \forall \psi \in \boldsymbol{\Omega} \tag{22}$$

Technical constraints of DGs and PV units for active power generation are shown by Eqs. (15) and (16). The mathematic calculations of State of Charge (SOC) level of ESS units are provided by Eqs. (17) and (18). The limitation of the energy level of the ESS is denoted by Eq. (19). The charging/discharging powers of the ESS are limited by Eqs. (20)–(21). Eq. (22) indicates that at each hour, if the ESS exchanges power with the network, it can either be charged or discharged, but not both simultaneously. As mentioned, the scheduling horizon is discretized into hourly intervals, and thus Δt is equal to 1 h. Accordingly, in the SOC equations, the time-step is explicitly replaced by the value of 1 to maintain a compact and consistent formulation.

In Eqs. (15), (16), (19) and (20), the presence of parameter s_i indicates that if bus i is out of service due to an event, the power generation of the DG and PV units, as well as the charging and discharging power of the ESS connected to that bus, must also be zero.

- Constraints of MES units:

$$E^{MES}_{b,t,\psi} = E^{MES}_{b,initial} + P^{MES}_{ch,b,t,\psi}\cdot \eta^{MES}_{ch,b} - \frac{P^{MES}_{dch,b,t,\psi}}{\eta^{MES}_{dch,b}} \forall b \in \boldsymbol{MES}, \forall \psi \in \boldsymbol{\Omega}, t = 1 \tag{23}$$

$$E^{MES}_{b,t} = E^{MES}_{b,t-1,\psi} + P^{MES}_{ch,b,t,\psi}\cdot \eta^{MES}_{ch,b}\cdot \Delta t - \frac{P^{MES}_{dch,b,t,\psi}\cdot \Delta t}{\eta^{MES}_{dch,b}} = E^{MES}_{b,t-1,\psi} + P^{MES}_{ch,b,t,\psi}\cdot \eta^{MES}_{ch,b} - \frac{P^{MES}_{dch,b,t,\psi}}{\eta^{MES}_{dch,b}} \forall b \in \boldsymbol{MES}, \forall \psi \in \boldsymbol{\Omega}, t \geq 2 \tag{24}$$

$$E^{MES}_{b,min} \leq E^{MES}_{b,t,\psi} \leq E^{MES}_{b,max} \forall b \in \boldsymbol{MES}, \forall t \in \boldsymbol{T}, \forall \psi \in \boldsymbol{\Omega} \tag{25}$$

$$P^{MES}_{ch,b,t,\psi} \leq P^{MES}_{b,max}\cdot u^{MES}_{ch,b,t,\psi} \forall b \in \boldsymbol{MES}, \forall t \in \boldsymbol{T}, \forall \psi \in \boldsymbol{\Omega} \tag{26}$$

$$P^{MES}_{dch,b,t,\psi} \leq P^{MES}_{b,max}\cdot u^{MES}_{dch,b,t,\psi} \forall b \in \boldsymbol{MES}, \forall t \in \boldsymbol{T}, \forall \psi \in \boldsymbol{\Omega} \tag{27}$$

$$u^{MES}_{ch,b,t,\psi} + u^{MES}_{dch,b,t,\psi} \leq 1 \forall b \in \boldsymbol{MES}, \forall t \in \boldsymbol{T}, \forall \psi \in \boldsymbol{\Omega} \tag{28}$$

Several bilinear terms appear in the proposed formulation, arising from the multiplication of binary and continuous variables. These terms are linearized using standard auxiliary-variable techniques as provided in Appendix A.

3.4. Objective functions

3.4.1. Total welfare of loads according to the utility functions

In a smart distribution power system, it is assumed that each user (or load) is equipped with an Energy Consumption Controller (ECC), integrated into their smart meter, which manages and regulates their electricity usage. These ECCs not only monitor individual consumption but also facilitate coordination among loads and with the energy providers and the Distribution System Operator (DSO). All ECC units are interconnected, as well as linked to the DSO, via a communication network, typically a local area network (LAN).

In a power distribution system, each load operates as an independent entity with its own behavior. The electricity demand can fluctuate depending on several factors, such as time of day, weather conditions, and electricity pricing. Additionally, the nature of the load—whether residential or industrial—significantly influences how they respond to changes in price. For instance, residential loads may react differently to pricing variations compared to industrial users. These diverse demand responses under varying pricing scenarios can be systematically modeled using the concept of utility functions, as established in microeconomic theory. The behavior of various loads can, in fact, be captured by assigning different utility functions to them. For each load or consumer, we denote the utility function as U(x,ω), where x represents the load's power consumption level, and ω is a parameter that may differ across loads and change over time. More precisely, the utility function quantifies the consumer's level of satisfaction as a function of their power consumption. The utility function needs to fulfill the following properties:

1) *Property I: Utility functions are essentially non-decreasing, meaning that loads always prefer to consume more electricity when available, up to their maximum allowable demand. Mathematically, this implies that:*

$$\frac{\partial U(x,\omega)}{\partial x} \geq 0 \tag{29}$$

2) *Property II*: *The marginal benefit of loads defined as* $V(x,\omega) = \frac{\partial U(x,\omega)}{\partial x}$ *should be a non-increasing function of* x. *Therefore, it can be written*:

$$\frac{\partial V(x,\omega)}{\partial x} \leq 0 \tag{30}$$

In other words, utility functions are concave, indicating that users' satisfaction increases and eventually saturates.

3) *Property III*: *It is necessary to prioritize loads according to their utility levels. In the presented formulation, it is assumed that for a given consumption level* x, *a higher value of* ω *corresponds to a higher utility* $U(x,\omega)$, *which can be written as*:

$$\frac{\partial U(x,\omega)}{\partial \omega} > 0 \tag{31}$$

4) *Property IV*: *We adopt the common assumption that zero power consumption yields zero utility, leading to*:

$$\partial U(0,\omega) = 0 \forall \omega > 0 \tag{32}$$

Although many types of utility functions satisfy Eqs. (29)–(32), in this paper, a quadratic utility function corresponding to linear decreasing marginal benefit is considered for loads as follows:

$$U(x,\omega) = \begin{cases} \omega x - \frac{a}{2}x^2 & \text{if } 0 \leq x \leq \frac{\omega}{a} \\ \frac{\omega^2}{2a} & \text{if } x \geq \frac{\omega}{a} \end{cases} \tag{33}$$

where, a is defined as a pre-specified parameter for loads. Sample utility functions based on Eq. (33) are plotted in Fig. 2.

To maintain the linearity of the proposed model, the utility function of each consumer for a predefined ω is represented as a piecewise linear function including three or five segments, as illustrated in Fig. 3. This approach allows us to approximate a general concave utility curve using multiple linear segments, while preserving the essential characteristics of diminishing marginal utility. By doing so, the users' preference is captured by the DSO for higher consumption levels up to a saturation point, without introducing non-linearity into the model. Each segment corresponds to a specific consumption level with an associated utility value, enabling the model to balance user satisfaction and resource allocation within a linear programming framework.

A load consuming x kW of electricity during an hour at a rate of π dollars per kWh incurs a cost of πx dollars per hour. Therefore, the welfare of each load defined by $W(x,\omega)$ can be expressed as:

$$W(x) = U(x) - \pi x \tag{34}$$

According to the above explanations, the first objective function maximizes the total welfare of loads based on their priority quantized by their utility function as given by Eq. (35):

$$OF_1 = \sum_{\psi\in\boldsymbol{\Omega}} \rho_\psi \sum_{i\in\boldsymbol{N}} \sum_{t\in\boldsymbol{T}} \left[U_i\left(P^d_{i,t,\psi}\right) - \pi_t P^d_{i,t,\psi} \right] \tag{35}$$

where, $U_i\left(P^d_{i,t,\psi}\right)$ is defined as the utility function of load at bus-i based on $P^d_{i,t,\psi}$ according to a piecewise linear function as shown in Fig. 3. It is important to note that since the utility function is unitless, the welfare function of loads is also unitless.

To model the linearized utility function, three binary variables $m^1_{i,t,\psi}$, $m^2_{i,t,\psi}$, $m^3_{i,t,\psi}$ and three continuous variables $\delta^1_{i,t,\psi}, \delta^2_{i,t,\psi}, \delta^3_{i,t,\psi}$ are used as described in Eq. (36).

$$\begin{aligned} U_i\left(P^d_{i,t,\psi},\omega_i\right) = \Big[& m^1_{i,t,\psi}\left(\delta^1_{i,t,\psi} \times u1_i\right) + m^2_{i,t,\psi}\left(\alpha^1_i \times u1_i + \delta^2_{i,t,\psi} \times u2_i\right) \\ & + m^3_{i,t,\psi}\left(\alpha^1_i \times u1_i + \alpha^2_i \times u2_i + \delta^3_{i,t,\psi} \\ & \times u3_i\right) \Big] P^{Load}_{i,t} \forall i \in \boldsymbol{N}, \forall t \in \boldsymbol{T}, \forall \psi \in \boldsymbol{\Omega} \end{aligned} \tag{36}$$

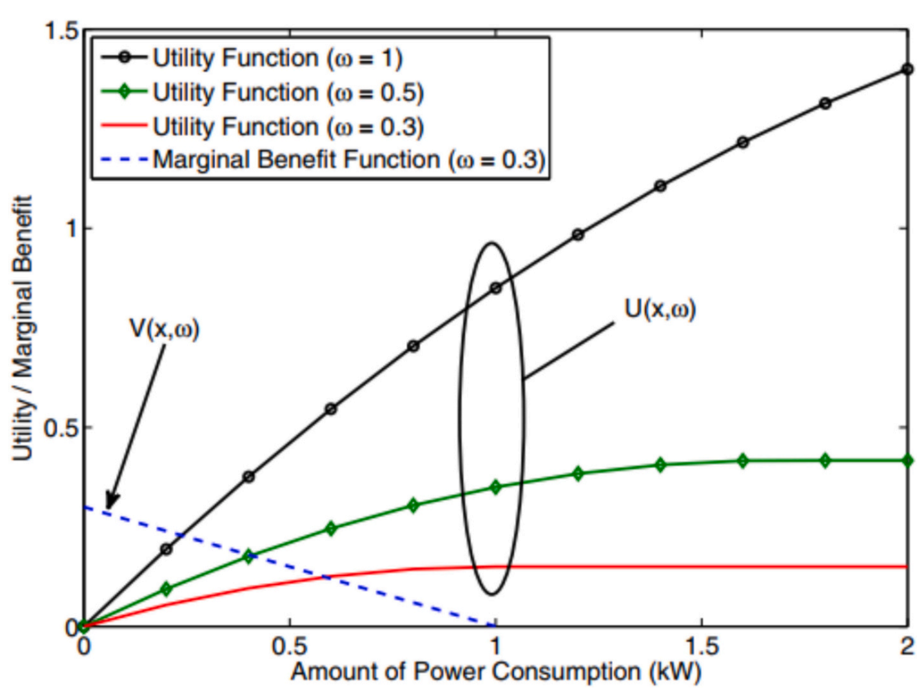

Fig. 2. Sample utility functions for loads with $a = 0.3$ and various ω.

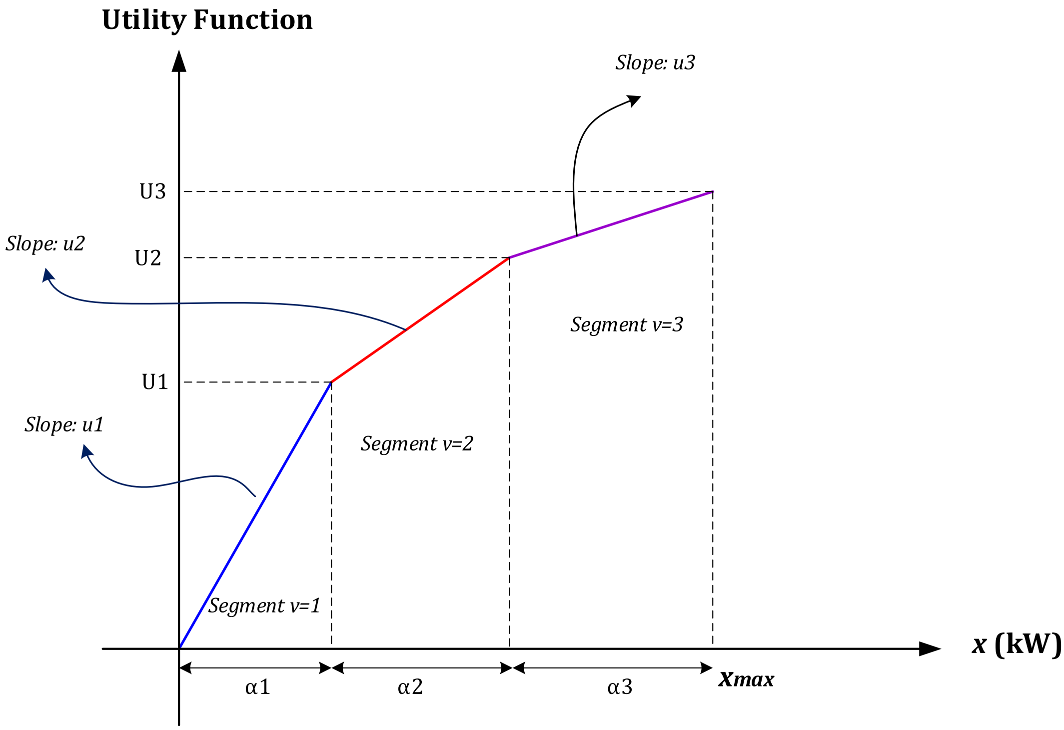

Fig. 3. A piecewise linear utility function used for loads.

$$P^{d}_{i,t,\psi} = \left[m^{1}_{i,t,\psi}\left(\delta^{1}_{i,t,\psi}\right) + m^{2}_{i,t,\psi}\left(\alpha^{1}_{i} + \delta^{2}_{i,t,\psi}\right) + m^{3}_{i,t,\psi}\left(\alpha^{1}_{i} + \alpha^{2}_{i} + \delta^{3}_{i,t,\psi}\right)\right] P^{Load}_{i,t} \forall i \in \boldsymbol{N}, \forall t \in \boldsymbol{T}, \forall \psi \in \boldsymbol{\Omega} \tag{37}$$

$$\delta^{v}_{i,t,\psi} \leq \alpha^{v}_{i} \; v = 1,2,3 \forall i \in \boldsymbol{N}, \forall t \in \boldsymbol{T}, \forall \psi \in \boldsymbol{\Omega} \tag{38}$$

$$m^{1}_{i,t,\psi} + m^{2}_{i,t,\psi} + m^{3}_{i,t,\psi} = 1 \forall i \in \boldsymbol{N}, \forall t \in \boldsymbol{T}, \forall \psi \in \boldsymbol{\Omega} \tag{39}$$

Eq. (37) represents the consumption at each bus based on the activated level of each segment in the piecewise linear utility function model. The limitation on the variables defined for the amount of load supplied in each segment is given by Eq. (38). As shown in Eq. (39), $m^{1}_{i,t,\psi}, m^{2}_{i,t,\psi}$ and $m^{3}_{i,t,\psi}$ are used to indicate that the utility function is represented in only one of the three defined segments. To linearize the product of variables in Eqs. (36)–(39), a similar method to that presented in Appendix A is utilized.

3.4.2. Operational cost during the restoration process

The restoration or operational cost encompasses the total budget needed to supply power from fossil fueled DGs and PV sources, cost of charging/discharging of ESSs along with the operational cost of MESs, as well as the cost of shed loads at various buses. Accordingly, the second objective function that should be minimized is defined in Eq. (40).

$$\begin{aligned} OF_2 = \sum_{\psi \in \boldsymbol{\Omega}} \rho_{\psi} \Bigg[& \sum_{i \in \boldsymbol{N}} \sum_{t \in \boldsymbol{T}} \Big(P^{DG}_{i,t,\psi} \times Price^{DG}_{i,t} + P^{PV}_{i,t,\psi} \times Price^{PV}_{i,t} \\ & + \left(P^{ESS}_{dch,i,t,\psi} + P^{ESS}_{ch,i,t,\psi}\right) \times Price^{ESS}_{i,t} + \left(P^{Load}_{i,t} - P^{d}_{i,t,\psi}\right) \times VOLL^{shed}_{i,t} \Big) \\ & + \sum_{b \in \boldsymbol{MES}} \sum_{t \in \boldsymbol{T}} \left(\left(P^{MES}_{dch,b,t,\psi} + P^{MES}_{ch,b,t,\psi}\right) \times Price^{MES}_{b,t} \right) \Bigg] \end{aligned} \tag{40}$$

In Eq. (40), $\left(P^{Load}_{i,t} - P^{d}_{i,t,\psi}\right)$ represents the amount of shed load at bus i, time t, and scenario ψ.

4. Optimization approach

The ε-constraint method in this paper is applied to solve the proposed multi-objective optimization problem. In the first step of this approach, a payoff table needs to be computed, which includes the optimal values obtained by individually optimizing each objective function. Once the payoff table is established, one objective is selected as the primary objective function, while the other is incorporated as a constraint [49]. This transformation allows the problem to be reformulated as a single-objective optimization model, subject to constraints given by Eq. (41):

$$\begin{aligned} & \max(OF_1) \\ & \text{Subject to}: \\ & OF_2 \leq \varepsilon \end{aligned} \tag{41}$$

Equal and unequal constraints

The single-objective optimization problem is solved iteratively for different values of ε, starting from the minimum value of OF_2 and progressing to its maximum. Each iteration yields an optimal solution, and the set of these solutions creates the Pareto optimal front of the multi-objective problem. To identify the most preferred solution from this set, a fuzzy satisfaction method is applied. This technique normalizes both conflicting objective functions, as described in Eqs. (42) and (43), enabling the selection of the best compromise solution. Eqs. (42) and (43) provide the fuzzification method for maximization and minimization objectives, respectively [50].

$$\mu^{k}_{i(i=1)} = \begin{cases} 0 & F^{k}_{i} \leq F^{min}_{i} \\ \dfrac{F^{k}_{i} - F^{min}_{i}}{F^{max}_{i} - F^{min}_{i}} & F^{min}_{i} \leq F^{k}_{i} \leq F^{max}_{i} \\ 1 & F^{k}_{i} \geq F^{max}_{i} \end{cases} \tag{42}$$

$$\mu_{i(i=2)}^{k} = \begin{cases} 1 & F_i^k \le F_i^{min} \\ \dfrac{F_i^{max} - F_i^k}{F_i^{max} - F_i^{min}} & F_i^{min} \le F_i^k \le F_i^{max} \\ 0 & F_i^k \ge F_i^{max} \end{cases} \tag{43}$$

The total membership function (i.e., the overall degree of optimality) for each Pareto optimal solution is calculated by combining the individual membership functions of the objective functions, weighted according to their respective importance factors (λ_i), as follows:

$$\mu^k = \sum_{i=1}^{2} \lambda_i \mu_i^k \tag{44}$$

The optimal restoration scheme is identified by ranking all alternatives according to the value of μ^k, as defined in Eq. (44). In this study, it is assumed that the objective functions have the same importance. Thus, the weighting factors λ_i are equal, i.e., 0.5.

It should be noted that Eqs. (42)–(44) jointly perform objective normalization, weighting, and compromise selection. Specifically, the payoff table provides the scaling bounds, Eqs. (42) and (43) normalize the conflicting objectives, and Eq. (44) identifies the final Pareto solution using a fuzzy satisfaction criterion with equal weights.

5. Simulation results and discussion

In this section, the proposed model is applied to a modified IEEE 33-bus distribution network as illustrated in Fig. 4. The model has been solved using the GUROBI solver within the GAMS environment, with a relative optimality gap set to 0.001%. Notably, the MG formation-based restoration approach is adaptable for post-disaster scenarios, as long as specific event consequences, such as line and bus outages, are accurately incorporated into the model. Four master control DG units are installed at buses 13 (with capacity of 400 kW), 20 (with capacity of 400 kW), 23 (with capacity of 300 kW), and 29 (with capacity of 300 kW). Thus, the maximum number of formable MGs is four. Additionally, three PV panels, each rated at 150 kW, are located at buses 9, 18 and 27. The network has a total active power demand of 70.14 MW during a 24-h scheduling period. An ESS unit is assumed to have a capacity of 50 kWh, with a maximum charging/discharging rate of 20 kW, an efficiency of 95%, and an initial SOC of 30%. Two MES units with a capacity of 100 kWh, a charging/discharging rate of 30 kW, an efficiency of 95%, and an initial SOC of 30% are also considered in the simulation. Tables 2 and 3 present the technical data and operating costs associated with DG units, PVs, ESSs, and MES units. The value of $VOLL_{i,t}^{shed}$ is assumed to be 10 $/kWh. The parameters of the load utility functions at different buses, as shown in Fig. 3, are provided in Table 4. The hourly rate of electrical energy in the distribution network is illustrated in Fig. 5.

Consider a load at bus 2 with a maximum demand of 100 kW. Based on the parameters reported in Table 4 (first row), the utility function is linearized using three segments with the following characteristics:

Segment 1 ($\alpha_1 = 0.563$): Maximum consumption level: 56.3 kW, Slope: $u_1 = 6$

Segment 2 ($\alpha_2 = 0.290$): Maximum consumption level: 29.0 kW, Slope: $u_2 = 3$

Segment 3 ($\alpha_3 = 0.147$): Maximum consumption level: 14.7 kW,

Table 2
The economic and technical data of DGs and PVs.

Component	Rated capacity (kW)	Location (Bus No.)	Generation cost ($/kWh)
DG	400	13, 20	0.08
	300	23, 29	0.08
PV	150	9, 18, 27	0.02

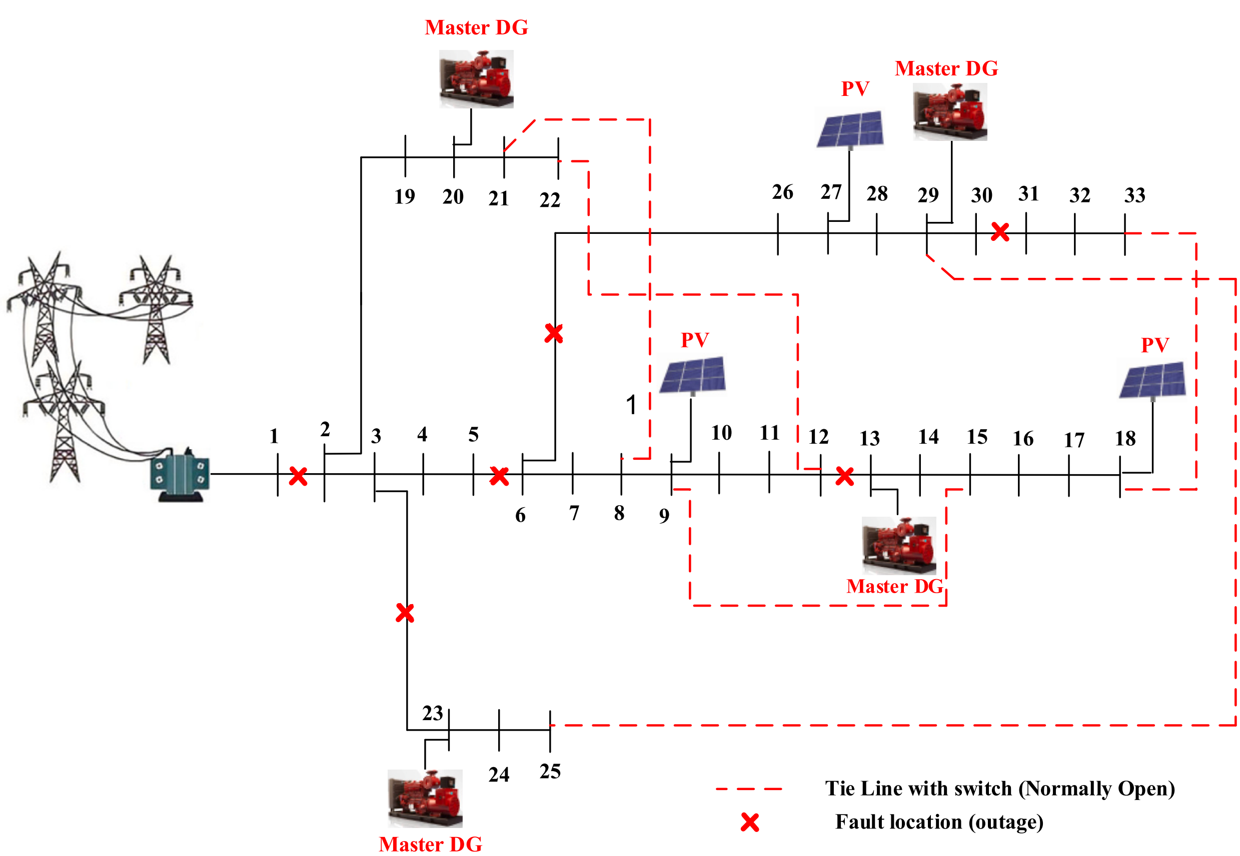

Fig. 4. The modified 33-bus distribution system with multiple faults.

Table 3
The economic and technical data of the ESS and MES units.

Component	Rated capacity (kWh)	Maximum charging/discharging power (kW)	Charging/discharging efficiency (%)	Initial SOC (%)	SOC limits	Operating cost ($/kWh)
ESS	50	20	95	30	20% - 90%	$Price_{i,t}^{ESS} = 0.01$
MES	100	30	95	30	20% - 90%	$Price_{b,t}^{MES} = 0.01$

Table 4
The parameters of the load utility functions.

Bus number	Maximum load consumption level in each segment as a percentage of the total maximum load (%)			Slope of each segment		
	α_i^1	α_i^2	α_i^3	$u1_i$	$u2_i$	$u3_i$
2	56.3	29.0	14.7	6	3	1
3	49.5	35.6	15.0	10	7	6
4	55.9	32.5	11.6	10	5	1
5	47.5	30.6	21.9	7	6	2
6	51.4	35.6	13.0	6	3	1
7	51.5	34.7	13.8	6	5	4
8	52.4	20.5	27.1	6	3	2
9	59.6	26.1	14.3	7	3	2
10	48.9	38.5	12.6	9	4	3
11	51.7	32.7	15.6	8	6	5
12	46.4	40.5	13.1	6	5	2
13	49.7	31.7	18.6	6	3	1
14	55.8	22.3	21.9	6	4	2
15	56.6	32.6	10.8	7	4	2
16	57.5	32.7	9.8	9	7	2
17	51.4	40.1	8.5	6	5	1
18	45.0	35.9	19.1	6	3	2
19	45.6	36.5	17.9	10	5	2
20	42.5	43.1	14.4	6	4	2
21	53.3	34.5	12.2	6	5	2
22	56.2	37.4	6.5	6	4	1
23	48.8	41.6	9.6	7	6	5
24	48.8	40.1	11.1	6	4	3
25	48.1	47.2	4.7	7	5	3
26	51.3	32.4	16.3	9	6	1
27	48.7	41.5	9.8	8	6	5
28	50.8	35.0	14.2	10	7	5
29	50.3	39.1	10.7	6	4	1
30	46.5	41.2	12.2	7	3	2
31	47.7	32.6	19.7	7	5	2
32	50.1	39.5	10.4	9	6	4
33	54.7	36.3	9.0	8	5	3

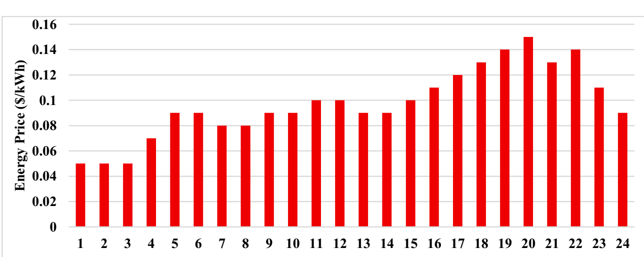

Fig. 5. Hourly energy price (tariff) in the distribution network.

Slope: $u_3 = 1$

These parameters correspond to a decreasing marginal utility, which is consistent with the concavity requirement of utility functions derived from Eq. (33). Moreover, the higher slope in the first segment reflects critical consumption with high marginal benefit, while lower slopes in subsequent segments represent non-essential or flexible loads. The high slope in the first segment represents critical consumption (e.g., lighting, medical devices, and essential services), for which consumers derive high satisfaction per unit of energy. The second and third segments represent less critical and discretionary consumption with progressively lower marginal benefits.

To address the uncertainty associated with PV sources, 1000 scenarios for a 24-hour scheduling horizon are initially generated using the Monte Carlo simulation method as described in [51]. Subsequently, the backward reduction technique is applied to select 5 representative scenarios for inclusion in the model. Two disaster scenarios are considered for the test system.

In this study, disaster impacts are modeled using predefined deterministic outage scenarios. The purpose is not to predict the component failure probabilities, but to assess the performance and adaptability of the proposed restoration framework under severe post-event conditions. The damage scenarios are therefore selected as representative stress-test cases, while the proposed model can accommodate any number and combination of damaged lines and buses as input data.

5.1. First disaster scenario

In the first disaster scenario, multiple faults occur at lines 1–2, 5–6, 12–13, 3–23, 6–26 and 30–31 during the tornado as marked by red crosses in Fig. 4. Thus, the HV/MV substation has been disconnected from the distribution networks. To explain the proposed model, three cases are defined as follows:

- Case 1: Single-objective operation based on minimizing restoration cost.
- Case 2: Single-objective operation based on maximizing total welfare of loads.
- Case 3: Multi-objective operation based on minimizing load shedding and minimizing operation cost.

5.1.1. Case 1: restoration cost-only optimization

In this case, network scheduling is carried out solely to minimize operational costs during the post-event restoration process. As illustrated in Fig. 6, the post-event network structure consists of four MGs formed under the given conditions. The supplied energy during the scheduling horizon is 37,078.8 kWh of which, 11985 kWh is related to MG1, 9600 kWh for MG2, 7101.3 kWh for MG3 and 8392.5 kWh for MG4. Also, the operational cost will be $ 333,291.25. As illustrated in Fig. 6, the MG formation method has successfully utilized all four DGs equipped with master control capabilities. Under this condition, the total load welfare, according to Eq. (35), is obtained as 219,311.41.

The optimization model determines the optimal location of grid connection for both MES units, as buses 23 and 24 in MG3. A technical reason for this selection becomes evident upon examining the load profile of this MG. The total peak load of MG3 including loads in buses 23 and 24 is 510 kW, while the capacity of only master DG located in MG3 is 300 kW. Therefore, installing two MES units in this MG and utilizing them by charging during off-peak hours and discharging during peak load periods justifies this selection.

The hourly scheduling of expected power generation by DG units and PVs during the post-event is plotted in Fig. 7. As observed, the highest production of generating units occurs at hour 12, while the lowest production is recorded at hour 4.

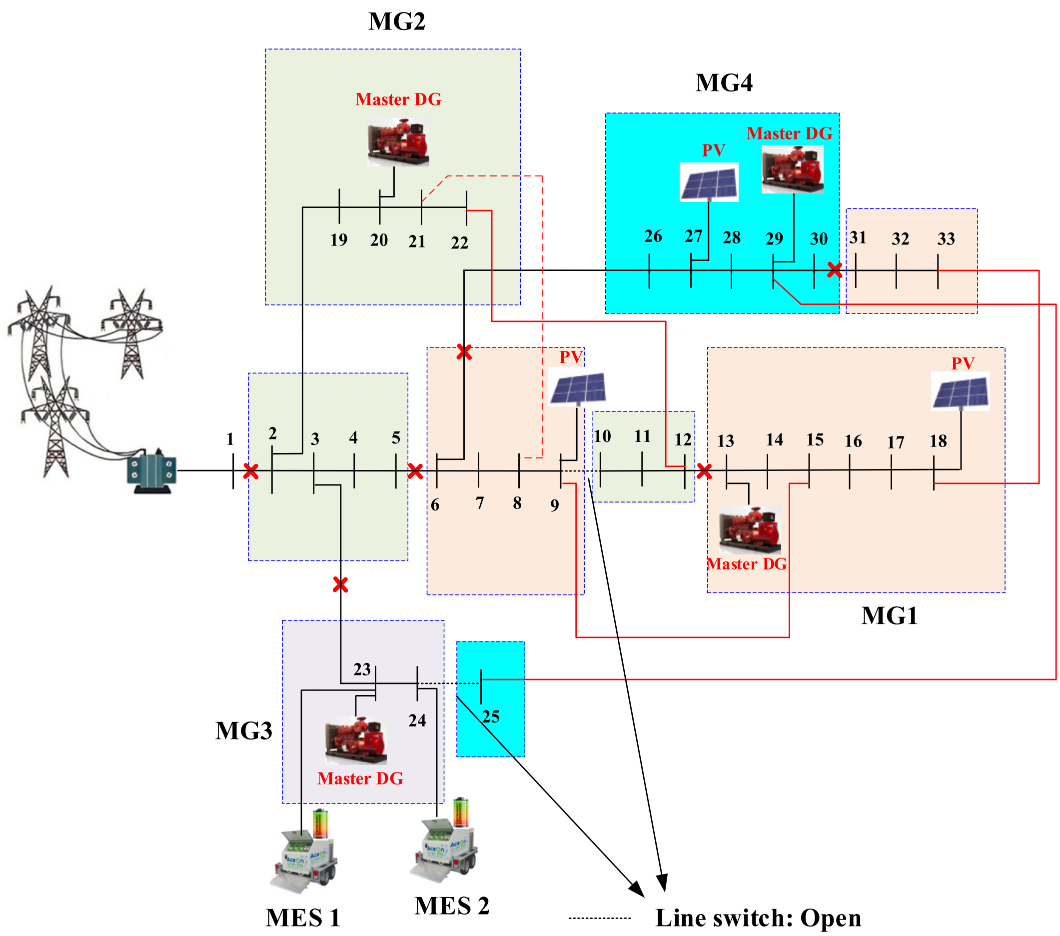

Fig. 6. Four MGs formation in the IEEE 33-bus distribution system with the optimal location of MES units in the first disaster scenario and case 1.

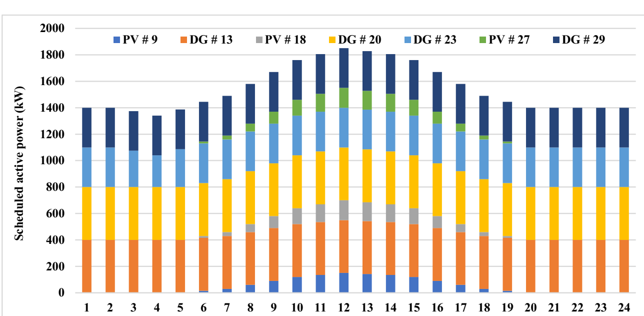

Fig. 7. Expected scheduling of active power production of DGs and PVs in the first disaster scenario and case 1.

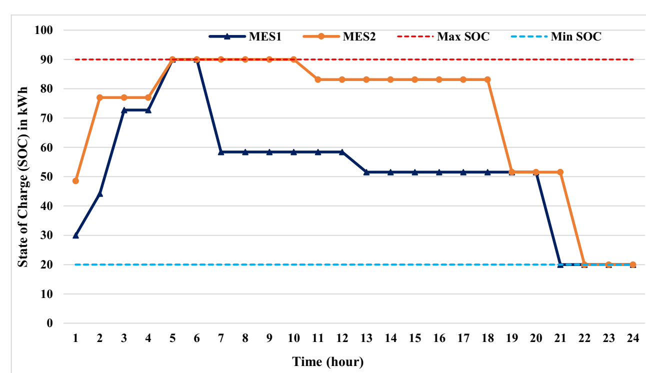

Fig. 8. The SOC of MES 1 and MES 2 in the first disaster scenario and case 1.

The State of Charge (SOC) or the stored energy level of MES 1 and MES 2 during the scheduling horizon is shown in Fig. 8. After connecting the MES units, the storage systems are charged during the early hours, remain nearly constant in th0.0e middle of the day, and discharge during peak load hours when the energy price in the grid is relatively high.

5.1.2. Case 2: total welfare-only optimization

In case 2, the restoration process is performed based on the maximization of the total welfare of loads during the post-event. The simulation results indicate that the MG formation structure in this case is identical to that of case 1, meaning the distribution network is divided into four MGs. However, the only difference lies in the optimal location

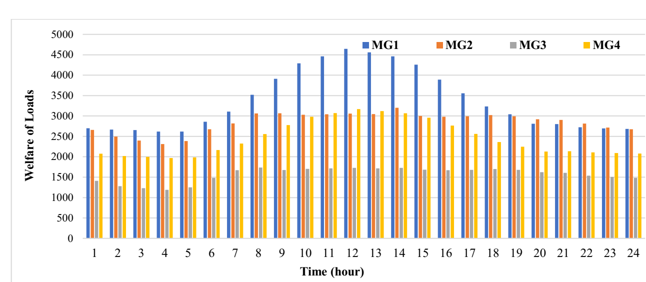

Fig. 9. The hourly total welfare of loads in each MG in the first disaster scenario and case 2.

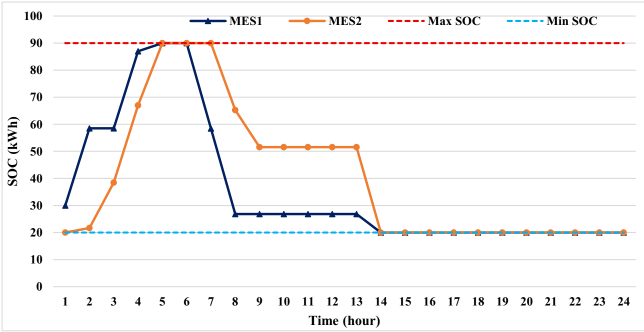

Fig. 10. The SOC of MES 1 and MES 2 in the first disaster scenario and case 2.

of the MES1, which has changed from bus 23 to bus 10. In other words, the optimal connection points of MESs 1 and 2 to the network are bus 10 in MG2 and bus 24 in MG3, respectively. Here, the total load welfare as the objective function becomes 245,445.69 while the operation cost will be calculated as $ 333,928.24. Fig. 9 illustrates the hourly values of the load welfare function in the four MGs. It is important to note that since the utility function is unitless, the welfare function of loads is also unitless. Moreover, the SOC of MES 1 and MES 2 during the scheduling horizon is plotted in Fig. 10.

Here, two complementary resilience-oriented indicators are introduced based on the post-event restoration performance. (i) Supplied Energy-Based Resilience Metric: the total supplied energy during the restoration horizon is used as a technical resilience metric, reflecting the system's capability to restore and sustain load supply after the disaster. Simulation results indicate that the total supplied energy increases from 33,195.6 kWh in the baseline case (without the proposed multi-microgrid formation model) to 37,078.8 kWh after applying the proposed approach, corresponding to an improvement of approximately 11.69%. (ii) Welfare-Based Resilience Metric: the total welfare of loads, derived from consumer utility functions, is employed as a socio-economic resilience metric, capturing not only the amount of restored load but also its priority and relative importance. The total welfare improves from 309,631.6 to 333,928.24, representing a 7.85% enhancement in socio-economic resilience.

Based on these metrics, quantitative resilience indices are defined as the ratio of post-event restored performance to the baseline damaged-network performance. Furthermore, a composite resilience index is calculated by equally weighting the energy-based and welfare-based indicators. The resulting composite index demonstrates an overall 9.77% improvement in system resilience, confirming the effectiveness of the proposed framework in enhancing post-disaster restoration performance from both technical and socio-economic perspectives. This improvement demonstrates that the proposed method enhances resilience not only by restoring more energy but also by prioritizing high-value and critical loads, thereby improving overall social welfare.

5.1.3. Case 3: multi-objective optimization

In this case, the scheduling process for restoration focuses on both objective functions, i.e., maximizing the total welfare of loads and minimizing restoration costs. Initially, the pay-off table is determined for the two objective functions in order to establish normalized values of pareto solutions based on the fuzzification method. These values presented in Table 5 are derived by solving each objective function separately. Based on the main problem formulation and the multi-objective optimization framework, this study employs the ε-constraint method to generate the Pareto frontier. In the proposed approach, total loads' welfare is selected as the main objective function, while the restoration cost is treated as an additional constraint. A total of 19 solution points is extracted along the Pareto front as presented in Table 6.

Table 5
Pay-off table of the ε-constraint method in the first disaster scenario and case 3.

Objective function	Total load welfare	Restoration cost in $
Total load welfare maximization	245,445.69	333,928.24
Restoration cost minimization	219,311.41	333,291.25

Table 6
Pareto frontier solutions for the IEEE 33-bus distribution network in the first disaster scenario and case 3.

Alternative	OF_1 (total welfare of loads)	OF_2 (total restoration cost in $)	μ_1^k	μ_2^k	$\mu^k = 0.5\mu_1^k + 0.5\mu_2^k$
1	245,445.69	333,928.24	1.0	0.0	0.5
2	245,431.31	333,915	0.9994	0.0208	0.5101
3	245,325.7	333,850	0.9954	0.1228	0.5591
4	245,329.82	333,835	0.9956	0.1464	0.5710
5	245,339.36	333,800	0.9959	0.2013	0.5986
6	245,351.71	333,750	0.9964	0.2798	0.6381
7	245,361.03	333,700	0.9968	0.3583	0.6775
8	245,363.83	333,685	0.9969	0.3819	0.6894
9	245,370.36	333,650	0.9971	0.4368	0.7170
10	245,379.68	333,600	0.9975	0.5153	0.7564
11	245,383.39	333,580	0.9976	0.5467	0.7722
12	245,388.92	333,550	0.9978	0.5938	0.7958
13	245,397.94	333,500	0.9982	0.6723	0.8352
14	245,406.96	333,450	0.9985	0.7508	0.8746
15	245,415.98	333,400	0.9989	0.8293	0.9141
16	245,419.59	333,380	0.9990	0.8607	0.9298
17	245,425.01	333,350	0.9992	0.9078	0.9535
18	**245,431.48**	**333,305**	**0.9995**	**0.9784**	**0.9889**
19	219,311.41	333,291.25	0.0	1.0	0.5

As shown in Table 6, the highest μ^k is achieved at point 18. At this point, the restoration cost is $333,305, and the total load welfare amounts to 245,431.48. The selected Pareto solution offers the most balanced trade-off between the two objectives. Based on the selected optimal Pareto point, the corresponding network is similar to case 1, as depicted in Fig. 6. Furthermore, the optimal connection points of MESs 1 and 2 to the network are buses 23 and 24 in MG3, respectively. Fig. 11 illustrates the Pareto front obtained from the ε-constraint method for the first disaster scenario, where each point corresponds to one solution listed in Table 6.

5.2. Second disaster scenario

In the second disaster scenario, multiple faults occur at lines 1–2, 12–13, 2–19, as well as at bus 6 during the tornado, as marked by red crosses in Fig. 12. In this state, similar to the first disaster scenario, the maximum number of formable MGs will be four. In addition, it is assumed that a fixed battery ESS with a rated capacity of 50 kWh, a charging/discharging rate of 20 kW, and an initial SOC of 30%.is connected to bus 32. Similar to the first disaster scenario, two MES units are available to the DSO, and it is necessary to determine their optimal locations for connection to the network. Here, the scheduling process for restoration focuses on both objective functions. The pay-off table is determined for the two objective functions in order to compute normalized values of the Pareto set based on the fuzzification method. These values provided in Table 7 are derived by solving each objective function separately. As reported in Section 5.1.3, the multi-objective optimization framework is solved by the ε-constraint method to generate the Pareto frontier. In the proposed approach, total loads' welfare is selected as the main objective function, while the restoration cost is treated as an additional constraint. A total of 9 solution points is extracted along the Pareto front as presented in Table 8.

As shown in Table 8, the highest μ^k is achieved at point 2. The selected Pareto solution offers the most balanced trade-off between the two objectives. Based on the selected optimal Pareto point, the corresponding network configuration is depicted in Fig. 12. Furthermore, the optimal connection points of MESs 1 and 2 to the network are buses 7

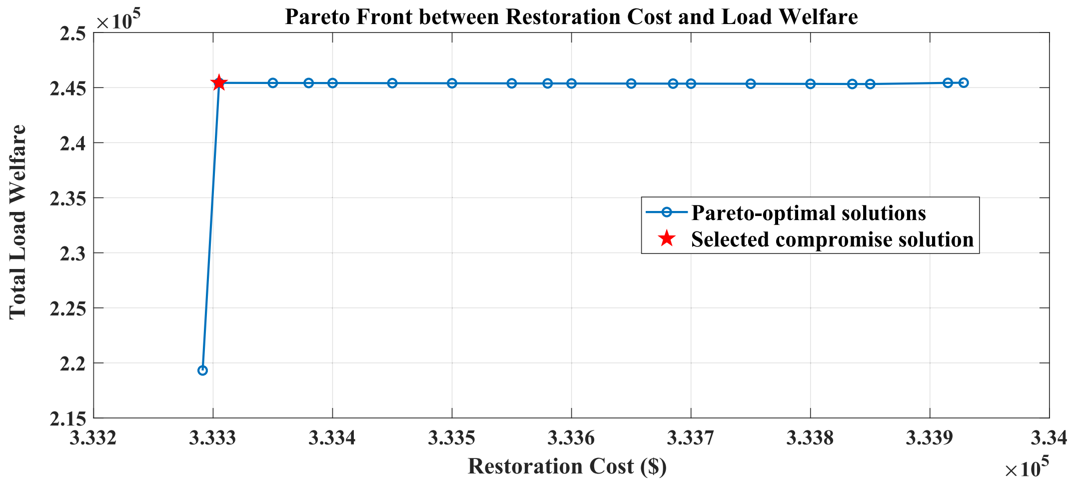

Fig. 11. Pareto optimal solutions for the first disaster scenario and case 3.

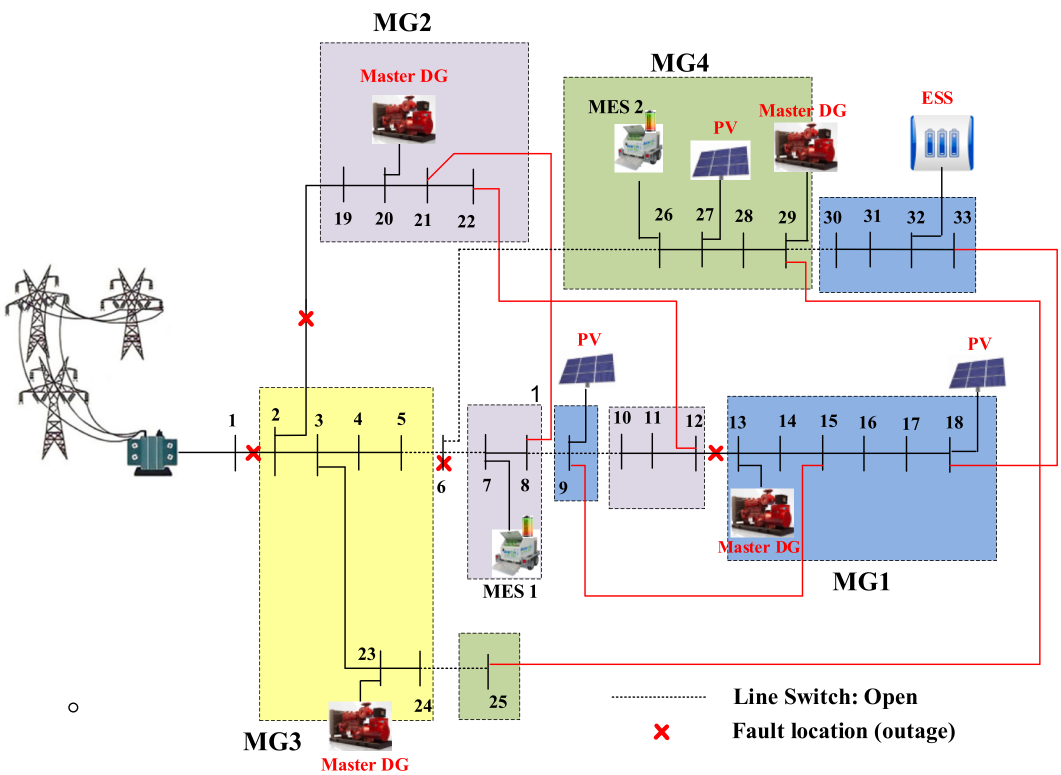

Fig. 12. MGs formation in the IEEE 33-bus distribution system with the optimal location of MES units in the second disaster scenario.

Table 7
Pay-off table of the ε-constraint method in the second disaster scenario.

Objective function	Total load welfare	Restoration cost in $
Total load welfare maximization	248,815.324	321,025.068
Restoration cost minimization	222,056.565	320,811.287

and 26 in MG2 and MG4, respectively.

When the restoration process is performed based on the maximization of total welfare of loads during the post-event (point 9 in Table 8), the simulation results indicate that the MG formation structure is identical to that in Fig. 12. However, the optimal connection of the MES 1 and MES 2 would be at buses 2 and 20, respectively. The SOC of MES 1 and MES 2 along with the fixed ESS during the scheduling horizon is plotted in Fig. 13.

Simulation results show that the supplied energy increases from 30,834.3 kWh to 37,177.5 kWh, corresponding to an improvement of approximately 20.57%. In addition, the total welfare improves from 241,919.6 to 248,581.02, indicating a 2.75% enhancement in socio-economic resilience. The composite resilience index is also calculated by equally weighting both indicators, resulting in an overall resilience improvement of approximately 11.66%. These definitions and results have been incorporated into the revised manuscript to quantify resilience enhancement explicitly.

Fig. 14 plots the Pareto front obtained from the ε-constraint method for the second disaster scenario, where each point corresponds to one solution listed in Table 8.

At the end, a brief computational performance analysis is provided in Table 9. The problem size is reported as the number of equations,

Table 8
Pareto frontier solutions for the IEEE 33-bus distribution network in the second disaster scenario.

Alternative	OF_1 (Total welfare of loads)	OF_2 (Total restoration cost)	μ_1^k	μ_2^k	$\mu^k = 0.5\mu_1^k + 0.5\mu_2^k$
1	222,056.565	320,811.287	0	1	0.5
2	**248,581.022**	**320,840**	**0.9912**	**0.8657**	**0.9285**
3	248,651.607	320,870	0.9939	0.7254	0.8596
4	248,701.645	320,900	0.9958	0.5850	0.7904
5	248,742.356	320,930	0.9973	0.4447	0.7210
6	248,784.369	320,960	0.9988	0.3044	0.6516
7	248,806.066	320,990	0.9997	0.1640	0.5818
8	248,814.480	321,010.092	1.0000	0.0701	0.5350
9	248,815.324	321,025.068	1	0	0.5

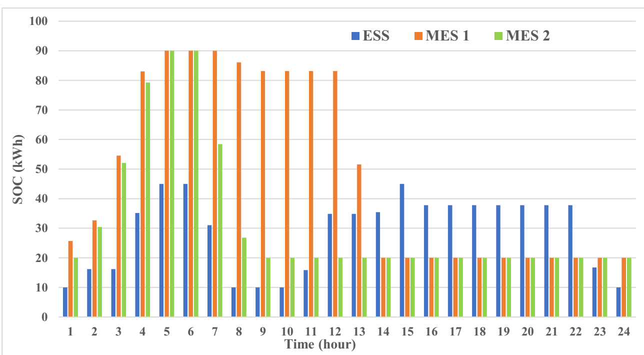

Fig. 13. The SOC of MES 1, MES 2 and ESS in the second disaster scenario obtained by optimization (maximization) of total welfare of loads.

variables, and discrete variables, along with solution times and optimality gaps. Results show that the proposed MILP model is computationally tractable for the IEEE 33-bus system, achieving zero relative optimality gap in all single-objective cases and near-zero gap for the ε-constraint-based multi-objective formulation. The number of ε-iterations and total computational time required to generate the Pareto front are also reported to clarify scalability and convergence behavior. All simulations were executed in the GAMS 28.2 environment using the GUROBI solver on a workstation equipped with an Intel Core i5-4210U CPU, 6.00 GB RAM, and a 64-bit operating system.

5.2.1. Sensitivity analysis

A sensitivity analysis is performed to examine how MES factors including the number of MES units and their rated capacity influence the outcomes discussed in the earlier subsection regarding the second disaster scenario. Table 10 presents the corresponding results of this analysis based on the single objective optimization of restoration cost and total loads welfare, separately. The optimization results indicate that the presence of MES reduces network restoration costs after an incident and improves the overall welfare of the loads. The results of the sensitivity analysis demonstrate that MES parameters, particularly energy capacity, have a significant impact on both the restoration cost and the welfare of loads. To better understand these effects, it is essential to interpret how different deployment strategies modify the balance between operational efficiency and consumer satisfaction.

MES Capacity: As shown in Table 10, increasing MES capacity from 50 kWh to 100 kWh yields clear improvements in welfare (up to +350 equivalent consumption) and cost reduction (up to −190 USD), illustrating that capacity is the dominant parameter in resilience-oriented MES planning. This behavior also reflects the fact that high-capacity MES units are more effective in covering long-duration shortages, resulting in both economic and social benefits.

Number of MES Units: Changing the number of MES units while keeping the total installed capacity fixed results in minor improvements. This suggests that splitting capacity across two units (e.g., 2×50 kWh instead of 1×100 kWh) does not significantly influence optimal welfare or cost.

Overall, the sensitivity analysis demonstrates that increasing the rated capacity of MES units yields a more pronounced improvement in

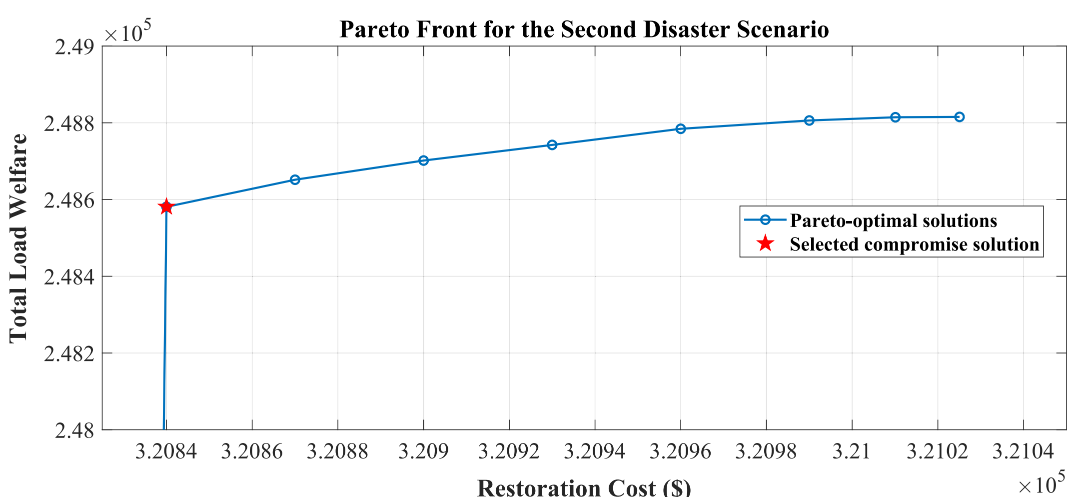

Fig. 14. Pareto optimal solutions for the second disaster scenario.

Table 9
Computational performance report for all disaster scenarios.

Disaster scenario	Objective	No. of equations	No. of variables	No. of binary variables	Solver time (s)	No. of runs	Relative gap
First scenario: case 1	Cost minimization	65,060	26,196	3078	230.5	1	0.0
First scenario: case 2	Welfare maximization	65,060	26,196	3078	204.5	1	0.0
First scenario: case 3	Multi-objective (ε-constraint)	65,060	26,196	3078	208.3–234.4	19	0.0
Second scenario	Multi-objective (ε-constraint)	84,741	32,817	3242	367.1–390.4	9	0.0

Table 10
Sensitivity analysis for the 33-bus distribution network considering the variation of MES parameters in the second disaster scenario.

Objective function	2 MES units with a capacity of 100 kWh	A MES unit with a capacity of 100 kWh	2 MES units with a capacity of 50 kWh	A MES unit with capacity of 50 kWh	Without MES	Without MES and ESS
Total load welfare maximization	248,815.324	248,667.018	248,667.627	248,566.348	248,458.389	248,367.49
Restoration cost minimization	320,811.287	320,906.19	320,906.192	320,953.645	321,001.097	321,048.55

both total welfare and restoration cost reduction compared to merely increasing the number of MES units with the same total capacity. This finding indicates that energy availability and discharge duration play a more critical role in post-disaster restoration than spatial redundancy under the considered scenarios.

To further investigate the robustness of the proposed restoration framework, a sensitivity analysis is conducted on the DG generation cost and MES prices for the second disaster scenario, as reported in Table 11. The results show that the total load welfare remains unchanged across all tested DG and MES operating cost levels. Although higher DG generation and MES costs increase the total restoration cost, the presence of MES units enables the system to preserve the same welfare level by shifting energy supply temporally and supporting critical loads during high-cost periods. This highlights the complementary role of MES in enhancing both economic robustness and resilience of the proposed framework.

6. Conclusion

This paper presented a comprehensive resilience-oriented post-disaster restoration model for smart distribution systems based on dynamic microgrid (MG) formation and optimal deployment of MES units. A multi-objective optimization framework was developed to maximize load welfare, quantified through utility functions, and minimize restoration costs using a MILP-based ε-constraint approach. Numerical results obtained from the IEEE 33-bus test system demonstrate that the proposed framework can effectively balance social and economic objectives during post-disaster restoration. In the first scenario disaster, the proposed model formed four MGs using four master DGs. Three operating cases were tested:

- Under case 1 (cost minimization only), the restoration cost was minimized at $333,291.25, supplying 37,078.8 kWh, with a total load welfare of 219,311.41.
- Under case 2 (welfare maximization only), total welfare increased to 245,445.69 with a slight increase in cost to $333,928.24, indicating a trade-off between economic and social objectives.
- In case 3 (multi-objective), the optimal Pareto point (alternative 18) provided a balanced solution with welfare of 245,431.48 and a cost of $333,305, achieving over 99.9% of maximum possible welfare while keeping costs near the minimum.

In the second scenario disaster, a similar approach led to the optimal restoration scheme with 248,581.022 of welfare and a cost of $320,840 (alternative 2), representing the best trade-off among 9 Pareto-optimal solutions.

Across both scenarios, the dynamic placement of MES units significantly enhanced restoration efficiency by enabling peak shaving and supporting under-capacity MGs. The strategic relocation of MES units—particularly to MGs with load-generation imbalances—proved crucial for optimal system performance. A sensitivity analysis was performed to examine how MES factors influence the outcomes in the second disaster scenario. The sensitivity analysis confirmed that increasing the rated capacity of MES units significantly enhances both restoration cost reduction and load welfare improvement. However, increasing the number of MES units with the same total capacity has a negligible impact on the objective functions. From a practical perspective, the proposed model offers a decision-support tool for distribution system operators to prioritize load restoration based on consumer welfare rather than demand magnitude alone, while efficiently allocating mobile storage resources under extreme events.

Future research directions include integrating transportation network constraints for realistic MES mobility modeling, incorporating electric vehicle fleets as mobile energy resources, and extending the proposed framework using scalable solution techniques such as decomposition-based or hybrid heuristic–optimization methods to reduce computational complexity for larger-scale distribution networks. Also, it will be necessary to investigate adaptive and heuristic-enhanced ε-constraint strategies to improve scalability and to efficiently generate the Pareto-front for such large-scale distribution networks.

CRediT authorship contribution statement

Mohammad Toulabi: Validation, Resources, Investigation, Formal analysis, Data curation. **Mehdi Nikzad:** Writing – original draft, Supervision, Software, Conceptualization. **Abouzar Samimi:** Writing – review & editing, Writing – original draft, Project administration, Methodology, Investigation, Data curation. **Amin Samanfar:** Writing – review & editing, Writing – original draft, Software, Resources, Investigation.

Funding

No funding was provided for this research.

Declaration of competing interest

The authors declare that they have no known competing financial interests or personal relationships that could have appeared to influence the work reported in this paper.

Table 11
Sensitivity of total welfare and restoration cost to DG fuel price and MES cost in the second disaster scenario.

Objective function	DG generation cost = 0.08 ($/kWh)			$Price_{b,t}^{MES}$ = 0.01 $/kWh		
	$Price_{b,t}^{MES}$ = 0.008 $/kWh	$Price_{b,t}^{MES}$ = 0.01 $/kWh	$Price_{b,t}^{MES}$ = 0.012 $/kWh	DG generation cost = 0.06 $/kWh	DG generation cost = 0.08 $/kWh	DG generation cost = 0.1 $/kWh
Total load welfare maximization	248,815.324	248,815.324	248,815.324	248,815.324	248,815.324	248,815.324
Restoration cost in $	321,024.202	321,025.068	321,025.934	320,353.068	321,025.068	321,697.068

Appendix A

This appendix presents the complete set of auxiliary-variable constraints used to linearize all bilinear terms appearing in the formulation, including products of binary–binary and binary–continuous variables. These constraints follow standard linearization techniques commonly adopted in MILP-based power system optimization models. As shown in Eq. (14), the multiplication of two binary variables $z_{i,m}$ and $X_{b,i}$ leads to a non-linear model. To linearize $z_{i,m}.X_{b,i}$, an auxiliary variable $g_{m,b,i} = z_{i,m}.X_{b,i}$ is utilized, which must satisfy the following constraints:

$$g_{m,b,i} \leq z_{i,m} \tag{A.1}$$

$$g_{m,b,i} \leq X_{b,i} \tag{A.2}$$

$$g_{m,b,i} \geq X_{b,i} + z_{i,m} - 1 \tag{A.3}$$

Also, in Eq. (14), the multiplication of a binary variable by a continuous variable must be linearized in order to obtain a linear model. Here, a positive continuous auxiliary variable is used to replace the product of the two original variables. For example, in the multiplication of $z_{i,\mathrm{m}}.P^{DG}_{i,t,\psi}$ the auxiliary positive variable $P^{aux-DG}_{m,i,t,\psi} = z_{i,\mathrm{m}}.P^{DG}_{i,t,\psi}$ is used along with the following constraints:

$$P^{aux-DG}_{m,i,t,\psi} \leq P^{DG}_{i,t,\psi} \tag{A.4}$$

$$P^{aux-DG}_{m,i,t,\psi} \leq z_{i,\mathrm{m}}.P^{DG}_{i,max} \tag{A.5}$$

$$P^{aux-DG}_{m,i,t,\psi} \geq P^{DG}_{i,t,\psi} - P^{DG}_{i,max}(1 - z_{i,m}) \tag{A.6}$$

Similarly, the remaining variable multiplications can be linearized.

Data availability

All data generated or analyzed during this study are included in this article. However, all datasets used during the current study are also available from the corresponding author upon reasonable request.

References

[1] M. Rouholamini, C. Wang, S. Magableh, X. Wang, Resiliency of electric power distribution networks: a review, J. Infrastruct. Preserv. Resil. 6 (1) (2025) 39, 2025/11/20, https://doi.org/10.1186/s43065-025-00154-y.

[2] J. Najafi, A. Peiravi, J.M. Guerrero, Power distribution system improvement planning under hurricanes based on a new resilience index, Sustain. Cities Soc. 39 (2018) 592–604, 2018/05/01, https://doi.org/10.1016/j.scs.2018.03.022.

[3] A. Gholami, T. Shekari, M.H. Amirioun, F. Aminifar, M.H. Amini, A. Sargolzaei, Toward a consensus on the definition and taxonomy of power system resilience, IEEE Access 6 (2018) 32035–32053, https://doi.org/10.1109/ACCESS.2018.2845378.

[4] R. Hemmati, H. Mehrjerdi, S.M. Nosratabadi, Resilience-oriented adaptable microgrid formation in integrated electricity-gas system with deployment of multiple energy hubs, Sustain. Cities Soc. 71 (2021) 102946, 2021/08/01, https://doi.org/10.1016/j.scs.2021.102946.

[5] P. Bajpai, S. Chanda, A.K. Srivastava, A novel metric to quantify and enable resilient distribution system using graph theory and Choquet integral, IEEE Trans. Smart Grid 9 (4) (2018) 2918–2929, https://doi.org/10.1109/TSG.2016.2623818.

[6] K.S.A. Sedzro, X. Shi, A.J. Lamadrid, L.F. Zuluaga, A heuristic approach to the post-disturbance and stochastic pre-disturbance microgrid formation problem, IEEE Trans. Smart Grid 10 (5) (2019) 5574–5586, https://doi.org/10.1109/TSG.2018.2887088.

[7] Y. Xu, C.C. Liu, K.P. Schneider, F.K. Tuffner, D.T. Ton, Microgrids for service restoration to critical load in a resilient distribution system, IEEE Trans. Smart Grid 9 (1) (2018) 426–437, https://doi.org/10.1109/TSG.2016.2591531.

[8] M. Zadsar, M. R. Haghifam, and S. M. Miri Larimi, "Approach for self-healing resilient operation of active distribution network with microgrid," IET Gener. Transm. Distrib., vol. 11, no. 18, pp. 4633–4643, 2017/12/01 2017, doi:https://doi.org/10.1049/iet-gtd.2016.1783.

[9] S. Biswas, M.K. Singh, V.A. Centeno, Chance-constrained optimal distribution network partitioning to enhance power grid resilience, IEEE Access 9 (2021) 42169–42181, https://doi.org/10.1109/ACCESS.2021.3065577.

[10] M. A. Gilani, A. Kazemi, and M. Ghasemi, "Distribution system resilience enhancement by microgrid formation considering distributed energy resources," Energy, vol. 191, p. 116442, 2020/01/15/ 2020, doi:https://doi.org/10.1016/j.energy.2019.116442.

[11] H. Momen, A. Abessi, S. Jadid, Using EVs as distributed energy resources for critical load restoration in resilient power distribution systems, IET Gener. Transm. Distrib. 14 (18) (2020) 3750–3761, 2020/09/18, https://doi.org/10.1049/iet-gtd.2019.1561.

[12] H. Momen, A. Abessi, S. Jadid, M. Shafie-khah, J.P.S. Catalão, Load restoration and energy management of a microgrid with distributed energy resources and electric vehicles participation under a two-stage stochastic framework, Int. J. Electr. Power Energy Syst. 133 (2021) 107320, 2021/12/01, https://doi.org/10.1016/j.ijepes.2021.107320.

[13] M. Alizadeh, M. Jafari-Nokandi, M. Shahabi, Resiliency-oriented islanding of distribution network in the presence of charging stations for electric vehicles, Int. Trans. Electr. Energy Syst. 30 (12) (2020) e12670, 2020/12/01, https://doi.org/10.1002/2050-7038.12670.

[14] J. Zhu, Y. Yuan, W. Wang, An exact microgrid formation model for load restoration in resilient distribution system, Int. J. Electr. Power Energy Syst. 116 (2020) 105568, 2020/03/01, https://doi.org/10.1016/j.ijepes.2019.105568.

[15] A. Samimi, M. Nikzad, A. Zakipour, Optimal sizing model of battery energy storage in a droop-controlled islanded multi-carrier microgrid based on an advanced frequency droop model, Sci. Rep. 15 (1) (2025) 2540, 2025/01/20, https://doi.org/10.1038/s41598-025-86368-2.

[16] Q. Shi, et al., Post-extreme-event restoration using linear topological constraints and DER scheduling to enhance distribution system resilience, Int. J. Electr. Power Energy Syst. 131 (2021) 107029, 2021/10/01, https://doi.org/10.1016/j.ijepes.2021.107029.

[17] F. Hafiz, B. Chen, C. Chen, A. Rodrigo de Queiroz, I. Husain, Utilising demand response for distribution service restoration to achieve grid resiliency against natural disasters, IET Gener. Transm. Distrib. 13 (14) (2019) 2942–2950, 2019/07/23, https://doi.org/10.1049/iet-gtd.2018.6866.

[18] M. Dabbaghjamanesh, A. Moeini, S. Senemmar, J. Zhang, Retracted: resiliency enhancement of distribution power grids using mobile marine power source, IEEE Trans. Ind. Appl. (2020) 1, https://doi.org/10.1109/TIA.2020.3007725.

[19] M.B. Siddique, J. Thakur, Assessment of curtailed wind energy potential for off-grid applications through mobile battery storage, Energy 201 (2020) 117601, 2020/06/15, https://doi.org/10.1016/j.energy.2020.117601.

[20] U. Berardi, E. Tomassoni, and K. Khaled, "A smart hybrid energy system grid for energy efficiency in remote areas for the army," Energies, vol. 13, no. 9, doi:https://doi.org/10.3390/en13092279.

[21] W. Shi, H. Liang, M. Bittner, Dynamic microgrid formation for resilient distribution systems considering large-scale deployment of mobile energy resources, Appl. Energy 362 (2024) 122978, 2024/05/15, https://doi.org/10.1016/j.apenergy.2024.122978.

[22] J. Zhong, et al., Resilient mobile energy storage resources-based microgrid formation considering power-transportation-information network interdependencies, Appl. Energy 389 (2025) 125716, 2025/07/01, https://doi.org/10.1016/j.apenergy.2025.125716.

[23] Y. He, G. Ruan, H. Zhong, Resilient distribution network with degradation-aware mobile energy storage systems, Electr. Pow. Syst. Res. 230 (2024) 110225, 2024/05/01, https://doi.org/10.1016/j.epsr.2024.110225.

[24] X. Guo, G. Miao, X. Wang, L. Yuan, H. Ma, and B. Wang, "Mobile energy storage system scheduling strategy for improving the resilience of distribution networks under ice disasters," Processes, vol. 11, no. 12, p. 3339 doi:https://doi.org/10.3390/pr11123339.

[25] M. Zhang, et al., Disaster management approaches for active distribution networks based on mobile energy storage system, Electr. Pow. Syst. Res. 239 (2025) 111242, 2025/02/01, https://doi.org/10.1016/j.epsr.2024.111242.

[26] H. Momen, S. Jadid, Resilience enhancement of power distribution system using fixed and mobile emergency generators based on deep reinforcement learning, Eng. Appl. Artif. Intel. 137 (2024) 109118, 2024/11/01, https://doi.org/10.1016/j.engappai.2024.109118.

[27] X. Dong, X. Xiong, D. Yang, S. Wang, and Y. Zhu, "Power supply resilience under typhoon disasters: a recovery strategy considering the coordinated dispatchable potential of electric vehicles and mobile energy storage," Processes, vol. 13, no. 6, p. 1638 doi:https://doi.org/10.3390/pr13061638.

[28] R. Xu, C. Zhang, D. Zhang, Z.Y. Dong, C. Yip, Adaptive robust load restoration via coordinating distribution network reconfiguration and mobile energy storage, IEEE Trans. Smart Grid 15 (6) (2024) 5485–5499, https://doi.org/10.1109/TSG.2024.3404776.
[29] T. Pan, et al., Resilience enhancement strategy for port distribution networks considering mobile energy storage, Electr. Pow. Syst. Res. 246 (2025) 111685, 2025/09/01, https://doi.org/10.1016/j.epsr.2025.111685.
[30] R.F. Alonso, A.C. Zambroni de Souza, Resilience of active networks with optimal mobile energy storage systems management, Electr. Pow. Syst. Res. 217 (2023) 109152, 2023/04/01, https://doi.org/10.1016/j.epsr.2023.109152.
[31] H. Saboori, Enhancing resilience and sustainability of distribution networks by emergency operation of a truck-mounted mobile battery energy storage fleet, Sustain. Energy Grids Netw. 34 (2023) 101037, 2023/06/01, https://doi.org/10.1016/j.segan.2023.101037.
[32] W. Abdulrazzaq Oraibi, B. Mohammadi-Ivatloo, S. H. Hosseini, and M. Abapour, "Multi microgrid framework for resilience enhancement considering mobile energy storage systems and parking lots," Applied Sciences, vol. 13, no. 3, p. 1285 doi:https://doi.org/10.3390/app13031285.
[33] M. Zamani Gargari, M. Tarafdar Hagh, S. Ghassem Zadeh, Preventive scheduling of a multi-energy microgrid with mobile energy storage to enhance the resiliency of the system, Energy 263 (2023) 125597, 2023/01/15, https://doi.org/10.1016/j.energy.2022.125597.
[34] Z. Wang, et al., A distributionally robust resilience enhancement model for transmission and distribution coordinated system using mobile energy storage and unmanned aerial vehicle, Int. J. Electr. Power Energy Syst. 152 (2023) 109256, 2023/10/01, https://doi.org/10.1016/j.ijepes.2023.109256.
[35] P.K. Ganivada, T.H.M. El-Fouly, H.H. Zeineldin, A. Al-Durra, Optimal siting and sizing of mobile-static storage mix in distribution systems with high renewable energy resources penetration, Electr. Pow. Syst. Res. 226 (2024) 109860, 2024/01/01, https://doi.org/10.1016/j.epsr.2023.109860.
[36] Y. Shen, et al., Mobile energy storage systems with spatial–temporal flexibility for post-disaster recovery of power distribution systems: a bilevel optimization approach, Energy 282 (2023) 128300, 2023/11/01, https://doi.org/10.1016/j.energy.2023.128300.
[37] Y. Wang, A.O. Rousis, D. Qiu, G. Strbac, A stochastic distributed control approach for load restoration of networked microgrids with mobile energy storage systems, Int. J. Electr. Power Energy Syst. 148 (2023) 108999, 2023/06/01, https://doi.org/10.1016/j.ijepes.2023.108999.
[38] M.-B. Niu, H.-C. Wang, J. Li, H. Liu, R. Yin, Coordinated energy dispatch of highway microgrids with mobile storage system based on DMPC optimization, Electr. Pow. Syst. Res. 217 (2023) 109119, 2023/04/01, https://doi.org/10.1016/j.epsr.2023.109119.
[39] M.J. Ghadi, D.K. Mishra, A. Azizivahed, L. Li, J. Zhang, Mobile compressed air energy storage for active distribution systems, Int. J. Electr. Power Energy Syst. 154 (2023) 109434, 2023/12/01, https://doi.org/10.1016/j.ijepes.2023.109434.
[40] S. Liu, et al., Joint operation of mobile battery, power system, and transportation system for improving the renewable energy penetration rate, Appl. Energy 357 (2024) 122455, 2024/03/01, https://doi.org/10.1016/j.apenergy.2023.122455.
[41] K. Tian, Y. Zang, J. Wang, X. Zhang, Electricity arbitrage for mobile energy storage in marginal pricing mechanism via bi-level programming, Int. J. Electr. Power Energy Syst. 162 (2024) 110330, 2024/11/01, https://doi.org/10.1016/j.ijepes.2024.110330.
[42] P. Sheikhzadehbaboli, A. Samimi, M. Ebadi, M. Bayat, A. Pirayesh, Frequency control in standalone renewable based-microgrids using steady state load shedding considering droop characteristic, Int. J. Electr. Power Energy Syst. 142 (2022) 108351, 2022/11/01, https://doi.org/10.1016/j.ijepes.2022.108351.
[43] T. Niknam, R. Azizipanah-Abarghooee, M.R. Narimani, An efficient scenario-based stochastic programming framework for multi-objective optimal micro-grid operation, Appl. Energy 99 (2012) 455–470, 2012/11/01, https://doi.org/10.1016/j.apenergy.2012.04.017.
[44] A. Khodaei, Resiliency-oriented microgrid optimal scheduling, IEEE Trans. Smart Grid 5 (4) (2014) 1584–1591, https://doi.org/10.1109/TSG.2014.2311465.
[45] T. Ding, K. Sun, C. Huang, Z. Bie, F. Li, Mixed-integer linear programming-based splitting strategies for power system islanding operation considering network connectivity, IEEE Syst. J. 12 (1) (2018) 350–359, https://doi.org/10.1109/JSYST.2015.2493880.
[46] S. Mousavizadeh, M.-R. Haghifam, M.-H. Shariatkhah, A linear two-stage method for resiliency analysis in distribution systems considering renewable energy and demand response resources, Appl. Energy 211 (2018) 443–460, 2018/02/01, https://doi.org/10.1016/j.apenergy.2017.11.067.
[47] M.A. Gilani, R. Dashti, M. Ghasemi, M.H. Amirioun, M. Shafie-khah, A microgrid formation-based restoration model for resilient distribution systems using distributed energy resources and demand response programs, Sustain. Cities Soc. 83 (2022) 103975, 2022/08/01, https://doi.org/10.1016/j.scs.2022.103975.
[48] T. Ding, Y. Lin, Z. Bie, C. Chen, A resilient microgrid formation strategy for load restoration considering master-slave distributed generators and topology reconfiguration, Appl. Energy 199 (2017) 205–216, 2017/08/01, https://doi.org/10.1016/j.apenergy.2017.05.012.
[49] M. Mesquita-Cunha, J.R. Figueira, A.P. Barbosa-Póvoa, New $\epsilon-$constraint methods for multi-objective integer linear programming: a Pareto front representation approach, Eur. J. Oper. Res. 306 (1) (2023) 286–307, 2023/04/01, https://doi.org/10.1016/j.ejor.2022.07.044.
[50] J. Aghaei, M.A. Akbari, A. Roosta, A. Baharvandi, Multiobjective generation expansion planning considering power system adequacy, Electr. Pow. Syst. Res. 102 (2013) 8–19, 2013/09/01, https://doi.org/10.1016/j.epsr.2013.04.001.
[51] M. Nikzad, A. Samimi, Integration of designing price-based demand response models into a stochastic bi-level scheduling of multiple energy carrier microgrids considering energy storage systems, Appl. Energy 282 (2021) 116163, 2021/01/15, https://doi.org/10.1016/j.apenergy.2020.116163.